Journal of Manufacturing Processes 101 (2023) 1275–1300

Contents lists available at ScienceDirect

Journal of Manufacturing Processes

journal homepage: www.elsevier.com/locate/manpro

Hybrid modelling method for the prediction and experimental validation of 3D printing resource consumption

Jimeng Yang [a], Ying Liu [b,*]

[a] Sino-European Institute of Aviation Engineering, Civil Aviation University of China, 300300 Tianjin, China
[b] School of Engineering, University of Glasgow, G12 8QQ Glasgow, United Kingdom

ARTICLE INFO

Keywords:
3D printing
G-codes
Resource consumption
Physical modelling
Data-driven modelling

ABSTRACT

In this study, a hybrid modelling scheme for 3D Printing (3DP) technology is proposed for predicting three resource consumption processes: production time, electric energy and material usage. First, the manufacturing process is classified into five machine operations: axial moving, material processing, unit heating, material feeding and auxiliary. Then, according to the machine behaviours, a Gantt chart and power profile (GP) diagram is generated for understanding operation processes and power variations. Based on the GP diagram, physical models and data-driven models are created for simulating the resource consumption level of each operation. The time and material consumed during part printing are physically modelled based on a computer numerical control (CNC) language: G-code. The power of each operation and the time consumed while preheating machine units are modelled through experimental measurements under different related process parameter values. The collected experimental data are regressed to obtain the functional relationships between the power, preheating time and process parameters. With the time and power submodels for all operations, the resource consumption models for the 3DP machine are assembled. To verify the effectiveness of this method, hybrid prediction modelling is demonstrated for two fused deposition modelling (FDM) machines, and the prediction accuracies are tested for real printing tasks. The proposed method can be adopted to other additive manufacturing processes by comprehensively considering related factors, including part geometries, process parameters, G-codes and machine behaviours.

1. Introduction

3D printing (3DP), as a typical additive manufacturing (AM) technology, has laid a milestone foundation for mass customisation due to its unlimited restrictions on the construction of complex and lightweight structures [1,2]. A typical 3DP process has three phases, as shown in Fig. 1: prefabrication, printing and postprocessing [3]. During the prefabrication phase, a computer-aided design (CAD) model is processed into a standard triangle language (STL) format. Then, based on process parameters, computer-aided manufacturing (CAM) slicer software implements built-in algorithms to slice the STL model into several layers and to plan the machine operations and material deposition toolpaths on each layer [1]. After that, the operations and toolpaths are programmed as G-codes, which is a general CNC programming language for AM and subtractive manufacturing (SM) technologies. Then, the process moves to the printing phase. By executing each command line in G-codes, machine units are activated to complete specific operations until the workpiece is delivered [4]. During the postprocessing phase, the workpiece is fine-finished by manually removing the support structure and by surface polishing to achieve the desired geometry [5].

Part quality and precision have long been the key evaluation criteria of manufacturing devices [6]. Most research is devoted to the evaluation of mechanical strength, fatigue limit and surface roughness, aiming at the optimisation of process parameters [7–9]. In recent decades, an evolution towards sustainable and environmentally friendly manufacturing has occurred [10]. As an emerging manufacturing technology replacing traditional processes, such as casting and milling, an effective assessment of AM sustainability from an environmental burden perspective is a crucial issue [11]. Preliminary studies have confirmed the higher resource demands of some AM processes than those of subtractive and bulk processes [12,13]. Hence, the resource consumption prediction of AM must be considered.

In the present work, a hybrid modelling method is proposed for predicting the time, energy and material consumptions of 3DP process. To achieve general prediction, we investigate the mainstream 3DP

* Corresponding author.
E-mail address: Ying.Liu@glasgow.ac.uk (Y. Liu).

https://doi.org/10.1016/j.jmapro.2023.06.030
Received 5 October 2022; Received in revised form 14 May 2023; Accepted 5 June 2023
Available online 13 July 2023

Nomenclature

Prediction modelling of time consumption

t	Total time consumption
t_{axis}	Time consumption of axial moving
t_{axis}^{w}	Axial moving time in working state
t_{axis}^{s}	Axial moving time in standby state
$\Delta X, \Delta Y, \Delta Z$	Axial motion distance for each toolpath on X-, Y-, and Z-axes, respectively
v_{xy}	Travelling/printing speeds on each toolpath on XY plane
v_{xy}^{min}	Minimum travelling/printing speeds
v_{xy}^{max}	Maximum travelling/printing speeds
v_z	Layer-switching speed on Z-axis
v_z^{min}	Minimum layer-switching speed
v_z^{max}	Maximum layer-switching speed
t_{mp}	Time consumption of material processing
t_{mp}^{p}	Material processing time in preheating state
t_{mp}^{w}	Material processing time in working state
T_{mp}^{0}	Present temperature of material processing
T_{mp}	Target temperature of material processing
T_{mp}^{max}	Maximum target temperature of material processing
ΔT_{mp}	Temperature difference from present temperature to target temperature of material processing
t_{uh}	Time consumption of unit heating
t_{uh}^{p}	Unit heating time in preheating state
t_{uh}^{w}	Unit heating time in working state
T_{uh}^{0}	Present temperature of unit heating
T_{uh}	Target temperature of unit heating
T_{uh}^{max}	Maximum target temperature of unit heating
ΔT_{uh}	Temperature difference from present temperature to target temperature of unit heating
T_0	Room temperature
t_{mf}	Time consumption of material feeding
t_{mf}^{w}	Material feeding time in working state
t_{mf}^{s}	Material feeding time in standby state
t_{layer}	Material feeding time per layer in BJ, PBF or SL technologies
N	Layer number
t_a	Time consumption of auxiliary operation
R^2	Goodness of fit of a regression model

Prediction modelling of energy consumption

E	Total energy consumption
E_{axis}	Energy consumption of axial moving
P_{axis}^{w}	Axial moving power in working state
P_{axis}^{s}	Axial moving power in standby state
E_{mp}	Energy consumption of material processing
P_{mp}^{p}	Material processing power in preheating state
P_{mp}^{w}	Material processing power in working state
E_{uh}	Energy consumption of unit heating
P_{uh}^{p}	Unit heating power in preheating state
P_{uh}^{w}	Unit heating power in working state
E_{mf}	Energy consumption of material feeding
P_{mf}^{w}	Material feeding power in working state
P_{mf}^{s}	Material feeding power in standby state
E_a	Energy consumption of auxiliary operation
P_a	Power of auxiliary operation

Prediction modelling of material consumption

M	Total material consumption
ΔV_{path}	Volume of material consumption per toolpath
ρ	Quoted material density
$\Delta \ell_{path}$	Material feed on each toolpath
r	Diameter of FDM material filament

G-code calculation for physical modelling.

C_N	Number of command lines in a G-code file

Prediction modelling of Monoprice MP Mini Delta FDM printer.

$t_{mp}^{w_1}$	Material processing time for the first layer in working state
$t_{mp}^{w_{rest}}$	Material processing time for the rest layers in working state
Δl_{xy}^{1}	Axial moving distance on XY plane for the first layer
v_{xy}^{1}	Travelling/printing speed on XY plane for the first layer
$P_{mp}^{w_1}$	Material processing power for the first layer in working state

Abbreviations

AM	Additive manufacturing
ANN	Artificial neural network
BJ	Binder jetting
CAD	Computer-aided design
CAM	Computer-aided manufacturing
CNC	Computer numerical control
DED	Direct energy deposition
EBM	Electron beam melting
FDM	Fused deposition modelling
GP	Gantt chart and power profile
ME	Material extrusion
MJ	Material jetting
PBF	Powder bed fusion
PLA	Polylactic acid
PLM	Polymerisation
SL	Sheet lamination
SLA	Stereolithography
SLS	Selective laser sintering
SM	Subtractive manufacturing
STL	Standard triangle language
3DP	3D Printing

technologies and classify five machine operations based on functions: axial moving, material processing, unit heating, material feeding and auxiliary. Correspondingly, the machine units that drive those machine operations are classified into five subsystems. Then, a Gantt chart and power profile (GP) diagram is formulated, which integrates the power profile of the printing process and the Gantt chart of the machine operations. Based on the GP diagram, the resource consumption of each operation is modelled. The modelling consists of two parts: 1) physical modelling based on G-codes; 2) data-driven modelling based on experimental data. Physical modelling sufficiently uses the toolpaths, printing speeds and material feeds encoded as G-codes to model the material usage and time consumed for axial motions. To model the resource consumption of the entire printing process, the resources consumed during machine preheating and standby should be considered. The preheating time and powers of the classified subsystems can be only modelled based on experimental data. Thus, during data-driven modelling, experiments are conducted to measure the preheating times and powers under different related process parameter values. The collected data are used for regressing the mathematical models of preheating times and powers. Finally, based on the GP diagram, the consumption models are assembled.

To verify the effectiveness of the proposed method, two real-world 3DP machines are used as test cases in this study: the Anycubic i3 Mega FDM printer and the Monoprice MP Mini Delta FDM printer. For

each machine, predictive models are developed by following the proposed method. Then, each machine is assigned two printing tasks using different process parameter values. The resource consumption of each printing task is predicted and compared with the actual consumption to calculate the prediction accuracy. The percent errors of time, energy, and material predictions reach 2.31%, 1.57 % and −8.05 % for the Anycubic machine and −2.48 %, 1.31% and −26.14 % for the Monoprice machine, respectively. The outcome of this research provides general guidance for manufacturers to model and predict the resource consumption of mainstream 3DP technologies and can potentially be applied to other AM and CNC manufacturing technologies.

The rest of this paper is organised as follows. In Section 2, recent research into AM resource consumption prediction is reviewed, followed by the research gaps and motivation. Section 3 presents a demonstration of the classifications of 3DP machine operations and subsystems. Then, the framework of the hybrid prediction modelling method is presented in Section 4. The mathematical models are developed and displayed in Section 5. The implementation of the proposed modelling method on two FDM machines is presented in Section 6, followed by the experimental validation of prediction accuracy in Section 7. Finally, a conclusion and future work are given in Section 8.

2. Background and motivation

With increasing public concern about resource scarcity, a comprehensive evaluation of environmental performance has become a major focus for advancing AM technologies. Resource consumption has been regarded as a direct measure for evaluating the environmental performance of AM [14]. In recent years, several research efforts have been attributed to predicting time, energy and material usage for various AM processes.

In the existing literature, time consumption models were mostly developed on subprocess levels [15]. For instance, the time of selective laser sintering (SLS) process modelled by [16] was divided into four phases: machine preparation, layer printing by laser beam, material feeding by metal powder roller and ending operations. The time of machine preparation and ending operations were fixed. The material feeding time was modelled as the layer numbers multiplied by the average time for feeding one layer's material. The layer printing time was modelled as the part volume divided by the average laser scanning rate. The time model of stereolithography (SLA) process was developed by [17]. Two time-consuming phases were identified: layer printing by ultraviolet light and axial moving for layer switching. The modelling of the layer printing time was based on the part volume and average laser scanning rate. The modelling of axial moving time was based on layer numbers and the time for switching one layer. Some research adopted machine learning to simulate the time model of AM processes. For instance, artificial neural network (ANN) was applied by [18] to train the time model of SLS process. The inputs of the Levenberg Marquardt learning algorithm included the build height, part volume and bounding box. The output was SLS process time. The prediction accuracy of the ANN model ranged from 2 % to 15 % errors. Grey theory was adopted to simulate the time model of FDM process in [19]. The method was used as a fuzzy mathematical tool to simulate the uncertain relationships between the time consumption and related factors: build height, part volume and bounding box. In the grey system, the inputs were the related factors, and the output was FDM process time. The prediction accuracy was within 10 % error.

Energy consumption models were generally developed by identifying the major energy consumers while printing and characterising the relationships between energy consumption and process parameters [14]. For instance, the energy of SLS process modelled by [21] was divided into three energy-consuming phases: machine warm-up, sintering and machine cool-down. The mean power of each phase was measured, and the energy was modelled as the mean power multiplied by the time consumed in each phase. The sintering time was the part volume divided by the average sintering time per unit volume of metal powder [20]. Binder jetting (BJ) process energy was modelled as the sum of energy for five units: infrared heater, uncap print head, sintering tool, curing tool and machine idle tool [22]. For the infrared heater and uncap print head, the energy was the product of the layer number, mean power and average printing time per layer. For curing and sintering tools, the energy was the sum of two states: heating and maintaining. The heating energy was the product of the temperature difference, total mass of material powder and average heating energy per unit mass for increasing the temperature by $1^{\circ}C$. The maintaining energy was an integral of power over runtime, where the power was a nonlinear function of thermal resistance, convection coefficient and temperature difference. For the machine idle tool, the energy was modelled as the machine standby power multiplied by the process time. The prediction accuracy ranged from 2 % to 7 % errors [22]. FDM process energy was modelled based on three energy-consuming units: electric drive, heater, and turbomachine. The mean power of each unit was measured and multiplied by its runtime to calculate the energy consumption. The prediction accuracy ranged from 1.6 % to 9.5 % errors [23]. SLA process energy modelled by [14] showed the accumulated energy of laser scanning for all layers. The layer number was calculated based on the part height and curing depth. The energy consumed on each layer was modelled as the laser power multiplied by its runtime. The runtime was estimated based on the laser scanning speed, contour lines and infill area on each layer. The prediction accuracy ranged from 5.85 % to 7.85 % errors. Electron beam melting (EBM) process was divided into seven phases: powder bed setup, build chamber cleaning, plate heating, beam alignment, building, cooling and vacuum generating [24]. The linear regression model of energy and runtime for each phase was obtained through experiments. The coefficient of each model (i.e., power of each phase) was found to be constant.

Research on AM material usage prediction is still scarce. In [22], the mass of metal powder and binder consumed in BJ process was modelled. The binder was used to bond the metal powder during printing, and its usage was the product of material density, volume used per layer and layer numbers.

According to the reviewed research, most studies focused on the consumption prediction for a single technology type, and the modelling methods were mainly based on the part volume and average resource demand per unit volume. Some methods adopted machine learning to

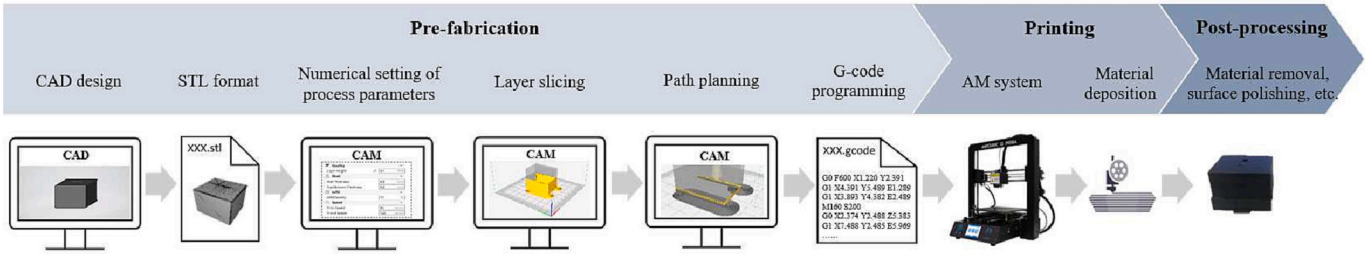

Fig. 1. Workflow of a typical 3DP process.

train consumption models; however, they neglected the impacts of process parameters on resource consumption. In fact, the part geometry and the numerical setting of process parameters determine the layer slicing and toolpath planning, thus affecting G-code programming. As the output from CAM, G-codes provide detailed commands for the machine operations and therefore decide the resource demands for fabricating the workpiece. In addition, machine behaviour is a factor affecting resource consumption. For instance, some machine units need to be heated to support printing. The preheating time and power are determined by the hardware characteristics and related to some process parameters, such as the heating temperature.

To propose a general prediction method with good accuracy, consumption modelling is supposed to consider the entire printing processes, machine behaviours and process parameters. G-code, as the key link between the prefabrication process and real-world printing process, provide detailed manufacturing information to assist in consumption modelling. To fill the above research gaps, we propose a hybrid modelling scheme to predict the time, energy and material consumptions of the 3DP process. The model integrates data-driven modelling based on experimental measurements and physical modelling based on G-codes, which makes full use of the toolpaths and machine unit schedules provided by G-codes and reduces the experimental workload on the machine. This method is not limited to only 3DP process but can also be applied to other AM and CNC manufacturing technologies.

3. Resource consumption-oriented and function-based classification method for 3DP technologies

Aiming at the general prediction method, we first investigate the mainstream 3DP technologies and find the common features of their printing processes. Regardless of which type of technology is adopted, a printing process is completed only through cooperative operations driven by multiple machine units with specific functions. In general, there are five functions: axial moving, material feeding, unit heating, material processing and auxiliary. By considering the common features, we classify the printing process into five operations based on the functions. The machine units are correspondingly classified into five functional subsystems. In the following subsections, details of this classification method are described, followed by the generation of a GP diagram based on the classified operations.

3.1. Classifications of machine operations and subsystems for mainstream 3DP technologies

Mainstream 3DP technologies are classified into seven categories: material extrusion (ME), direct energy deposition (DED), powder bed fusion (PBF), material jetting (MJ), Binder jetting (BJ), polymerisation (PLM) and sheet lamination (SL) [26]. A 3DP machine using any of these technologies has multiple machine units to cooperatively complete printing. Each unit performs its function to complete a specific operation, which is driven by a certain type of energy transformation. For instance, the Cartesian system of an ME machine can move the nozzle to a target coordinate. Electrical energy is transformed into mechanical energy to complete this operation.

From the perspective of CNC, there are five typical operations driven by the corresponding G-code commands, as shown in Table 1, namely axial moving, material feeding, unit heating, material processing and auxiliary. A command line consists of two parts: operational commands and parameters. The operational commands are used to drive the specific subsystem to begin the operation, followed by the parameters used to instruct the expected action. For instance, in command line “M109 S150”, operational command “M109” drives the material processing system to begin the heating operation; “S150” commands the system heating to the target temperature 150$^{\circ}C$.

Based on the five operations, the machine units are classified into five subsystems, as shown in Fig. 2. There are three types of energy transformations (i.e., electrical to mechanical energy, thermal energy and others) and states (i.e., working, preheating and standby) to drive the subsystem operations. In details, the axial moving operation has two states: working and standby. While working, the axial moving system drives the nozzle to a specific coordinate by following G-codes; otherwise, the system stands by. The material feeding operation has two states: working and standby. While working, the material feeding system deposits material along toolpaths or to feed materials on each layer; otherwise, the system stands by. The material processing operation has two states: preheating and working. Before depositing material, the material processing system is preheated to its target temperature. When the deposition begins, the system remains at target temperature to continuously process the material. Some 3DP technologies have unit heating systems to assist in material deposition. For instance, the heating of the build platform for MJ and ME is to adhere the workpiece base to the platform. During the preheating state, the system is preheated to its target temperature. During the working state, the platform maintains the temperature to continuously aid material deposition. The auxiliary operation remains in the working state to monitor and control the printing process. This classification method is generally applicable to any newly developed 3DP technology.

3.2. Resource consumption-oriented modelling based on machine operations and power profile

To model the time and energy consumptions of a 3DP process, the machine behaviour must be understood from three perspectives: 1) the machine operations needed for completing printing; 2) the subsystems used for driving the operations; and 3) the operation sequence during printing. The operations and corresponding subsystems are identified based on the energy-consuming machine units. The operations’ sequence is determined by the built-in algorithm provided by the slicer

Table 1
G-code commands for machine operations [27,28].

Operations	G-code commands	Operational commands	Definitions	Parameters	Definitions
Axial moving	G1/G0 F X Y G1/G0 F X Y G1/G0 F Z	G1, G0	Start linear axial moving	F X Y Z	Printing/travelling speed Endpoint coordinate of present toolpath on X-axis Endpoint coordinate of present toolpath on Y-axis Endpoint coordinate of present toolpath on *Z*-axis
Material feeding	G1 F X Y E	G1	Start material feeding	E	Present cumulative material feed
Unit heating	M190 S	M190	Heating from present to target temperature	S	Target temperature of unit heating
Material processing	M109 S	M109	Heating from present to target temperature	S	Target temperature of material processing
Auxiliary	None	Remain on-state during printing			

Operations		Axial moving	Material feeding	Unit heating	Material processing	Auxiliary
State	Working	√	√	√	√	√
	Preheating			√	√	
	Standby	√	√			
Energy transformations	Electrical to mechanical	√	√			√
	Electrical to thermal			√	√	
	Electrical to others					√
AM technologies	Sub-systems / Material forms	Axial moving system	Material feeding system	Unit heating system	Material processing system	Auxiliary system
Material Extrusion	Wire	Nozzle hotend	Build platform	Wire extruder	XYZ axes Cartesian system Delta system (3 parallel stepper motors) Polar system (radial and angular coordinates) Multi-axis robotic arm	Display unit User interface and connectivity Cooling fans Temperature sensor …
Direct Energy Deposition	Wire	Laser Electron beam Electric arc Plasma		Wire feeder Powder feeder	XYZ axes gantry system Multi-axis robotic arm X/Y/Z tables Rotary table Tilt-rotate trunnion	
Powder Bed Fusion	Powder	Laser Electron beam Thermal print head		Powder roller Powder supply platform Overflow bin	Laser scanner Build platform	
Material Jetting	Liquid	Ultraviolet light	Build platform Material container	Build material feeder Support material feeder	XY axes gantry system Build platform	
Binder Jetting	Powder	Inkjet nozzles		Powder roller New powder stock Overflow bin	XY axes gantry system Build platform	
Polymerisation	Sheet	Ultraviolet light Laser			Laser scanner Build platform	
Sheet lamination	Powder	Laser	Heated roller	Sheet roller	Laser scanner Build platform	

Fig. 2. Classifications of operations and subsystems for mainstream 3DP technologies.

software, and the starting time of each operation can be known from G-codes. To visually display the machine behaviour, a GP diagram is generated, which is used as the first-version model to abstract the machine behaviour. Fig. 3 presents an exemplary GP diagram of an FDM machine, which consists of two parts: Gantt chart and power profile.

In the Gantt chart, the starting time of each operation corresponds to its G-code command, and the duration depends on the hardware performance. For instance, at 00 m 45 s, the unit heating operation begins to preheat the build platform by following the command "M190". The time consumption of this preheating state depends on the temperature difference from present temperature to the target temperature, as well as the heating performance of the unit heating system. At 03 m 41 s, the build platform reaches its target temperature, and the material processing operation begins to preheat the nozzle hotend by following the command "M109". After the preheating state, both operations switch to the working state to maintain the target temperature until the end of printing. At 05 m 58 s, the material feeding and axial moving begin to deposit material by following the command "G1" or "G0".

The machine power profile is captured by using a power meter. The profile step change corresponds to the starting or state-switching of operations. For instance, from 00 m 45 s to 03 m 41 s, the power remains constant when the unit heating operation remains in the preheating state. From 03 m 41 s, the power is in the form of periodic pulses when the material processing operation begins.

The generation of a GP diagram can help to understand the machine operations and evaluate which time periods must be modelled to reduce

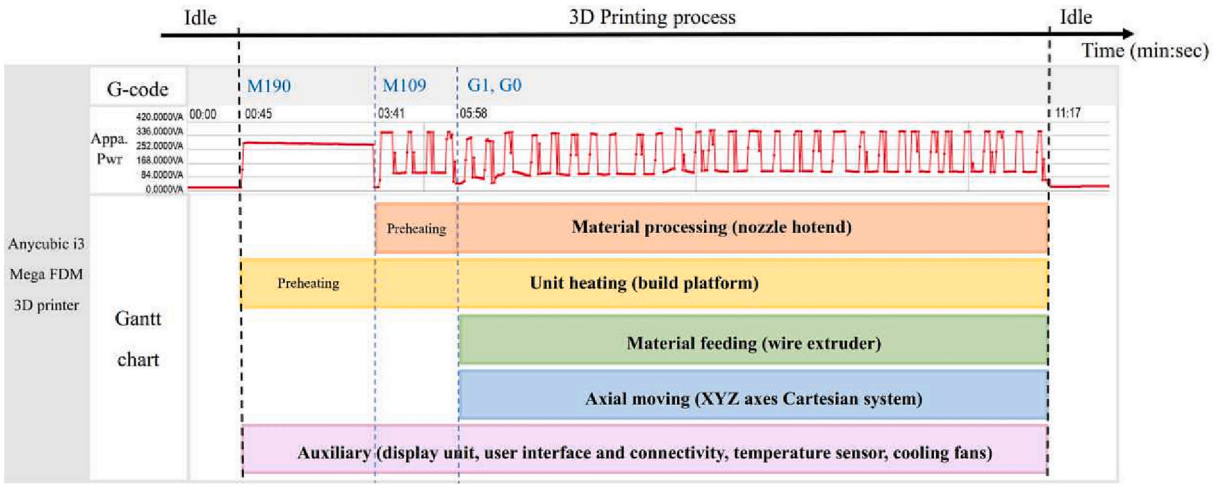

Fig. 3. Example GP diagram of the Anycubic i3 Mega FDM 3D printer [26].

the workload of time modelling. For instance, in Fig. 3, the five operations from 05 m 58 s to 11 m 07 s are simultaneous. When the time model of any operation in this period is obtained, the time consumption levels of other operations can be represented by this model. For non-simultaneous operations, the time must be modelled separately.

4. Framework of hybrid prediction modelling of 3DP resource consumption

In this study, a hybrid modelling method is proposed to predict the time, energy and material consumptions of the A3DP process. The method begins with the generated GP diagram to conduct prediction modelling. The framework of the modelling workflow is presented in, which includes three steps: environmental setup, prediction modelling and model assembly. Each step is described as follows.

4.1. Environmental setup for prediction modelling

The machine operations and subsystems are identified in the previous section. To model the resource consumption of a printing process, the G-codes used for commanding the machine operations must be identified. At the software level, the CAD design is imported into slicer software, where the values of process parameters are set by the machine user. Then, the design is sliced into multiple layers, and the toolpaths on each layer are planned and programmed as G-codes. The file of G-codes is used in the subsequent modelling step.

In addition, since the machine power and the preheating time of some machine units determine the total time and energy consumption levels, experiments are unavoidable for measuring those parameters. At the hardware level, a power meter connected to the 3DP machine must be prepared for the following data-driven model.

4.2. Hybrid prediction modelling of 3DP resource consumption

The hybrid prediction modelling transforms the first-version model (i.e., GP diagram) to the mathematical models of resource consumption, as shown in Fig. 4. The model includes two parts: physical modelling and data-driven modelling. Each part is described in the following subsections.

4.2.1. Physical modelling based on G-codes

G-codes provide toolpaths, speeds and material feeds for material deposition. This information is used to predict the time consumed for axial motions and the total material consumption, so called physical modelling based on G-codes. Here we take FDM technology as an example. In the command line “G1 F600 X17.156 Y26.687 E1.265”, the operational command “G1” drives the axial moving system to begin linear axial motion. “F600 X17.156 Y26.687” commands the axial moving from the previous coordinate to the target coordinate (X17.156 Y26.687) at a speed of 600 *mm*/*min*. With the coordinates and speeds, the time consumed for this motion can be calculated. “E1.265” commands the material feeding system to deposit filament materials during this motion. The total length of the deposited material is 1.265 *mm*. With the material feed, the mass of material consumption can be calculated. Details of this calculation method are found in Section 5.

4.2.2. Data-driven modelling based on experimental data

To predict the time and energy from the warming of the machine to the end of printing, the system preheating times and powers must be modelled. Since these parameters are not given in G-codes, their mathematical models are only developed based on experimental data, so called data-driven modelling. Table 2 lists the two types of parameters to be measured. According to G-code commands, it is assumed that the preheating time and the working powers of axial moving, mateiral feeding, unit heating and material processing are dependent to the

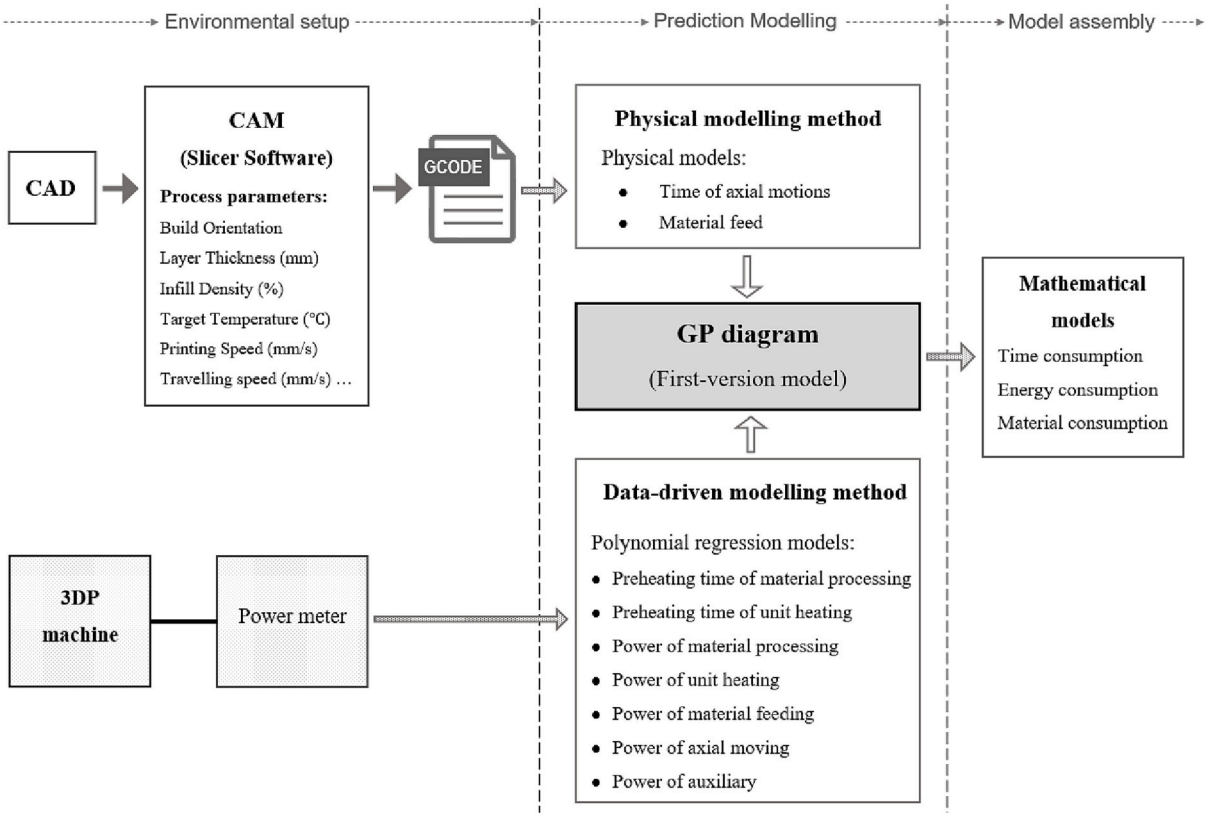

Fig. 4. Framework of the hybrid modelling method for 3DP resource consumption prediction.

Table 2
Experimental measurements for data-driven modelling [27,28].

Operations	Parameters		Related process parameter	G-code commands	Meanings
Axial moving	Dependent	Working power	v_{xy},v_Z	G1 Fv_{xy} X Y G1 Fv_z Z	Command axial moving on X- Y-axes at speed v_{xy}; Command axial moving on *Z*-axis at speed v_z.
	Independent	Standby power	None		
Material feeding	Dependent	Working power	v_{xy}	G1 Fv_{xy} E	Command material feeding at speed v_{xy}.
	Independent	Standby power	None		
Unit heating	Dependent	Preheating time Preheating power Working power	ΔT_{uh} T_{uh}	M190 ST_{uh}	Command system heating to target temperature T_{uh}.
Material processing	Dependent	Preheating time Preheating power Working power	ΔT_{mp} T_{mp}	M109 ST_{mp}	Command system heating to target temperature T_{mp}.
Auxiliary	Independent	Working power	None		

corresponding process parameters. The functional relationships need to be validated through experiments. The independent parameters, i.e., the standby powers and the working power of auxiliary operation, are unrelated to any process parameter, which can be directly measured as a constant.

For different machines, the preheating times and powers depend on the machine characteristics and process parameters. For instance, the unit heating system follows the command "M190 ST_{uh}" to initiate heating from the present temperature to the target temperature T_{uh}. The preheating time is determined by the temperature difference ΔT_{uh} and the heating performance of the unit heating system. In this study, we assume that the preheating time is functionally related to ΔT_{uh}, and the function coefficients are determined by the system heating performance. To validate this assumption, experiments are performed to measure the preheating time at different values of ΔT_{uh}. By adopting the regression analysis method, the collected experimental data are processed to derive the function coefficients. Additionally, it is assumed that the preheating power is related to both T_{uh} and the system heating performance. The functional relationship is derived in a similar manner.

With respect to the design of experiments, the corresponding G-code commands are manually programmed to command the machine to run each subsystem independently. For instance, for measuring the material processing power at different target temperatures T_{mp}, the G-code command "M109 ST_{mp}" is manually programmed, and the value of T_{mp} is randomly set within the boundary from the present temperature to the system's maximum temperature. During experimentation, each dependent parameter is measured by a power meter under different values of related process parameters. Note that we use the apparent power to estimate the power demand of the 3DP machine. The apparent power is a combination of the active power and the reactive power. The active power represents the electrical resistance power converted to mechanical and thermal energies, while the reactive power represents the inductive and capacitive powers used to form the magnetic and electric fields [30].

After the collection of experimental data, regression analysis is adopted to calculate the function coefficients. By using a polynomial regression tool, different degrees of polynomial functions are regressed, from which the most feasible function is selected as the regression model. According to [31], the function degree depends on the confidence bound of the coefficients. When the confidence bound of the highest order coefficient crosses zero, the polynomial function is overfitted, indicating that a low degree of polynomial function is more feasible. In addition, the statistical measure R-square (R^2) is calculated to estimate the goodness of fit of each regression model. The closer R^2 is to 1, the closer the sample points are to the regression curve, and the more significant the impact of process parameter on the measured dependent parameter [31,32].

4.3. Resource consumption model assembly

With the submodels of powers, preheating time and time consumed for axial motions, the time and energy models of each operation are formulated. From the GP diagram of the 3DP machine, the simultaneous operations and the independent operations are determined. For simultaneous operations, only one operation's time model must be formulated. This model is used for other operations and for modelling their energy consumption levels. For instance, the axial moving operation is generally simultaneous with the material feeding operation. Thus, the time consumed for axial motions is equal to the time consumed for material feeding, and their time models are the same. For independent operations, such as the preheating of the material processing system, the submodels of preheating time and energy can only be obtained through data-driven modelling.

With the time and energy models of all operations, the mathematical models of the total time and energy consumption levels are finally assembled according to the GP diagram. In terms of the material consumption, the model is formulated based on the submodel of the material feed per toolpath. Details of the above consumption models are presented in the next section. The notations used in prediction modelling are listed below.

5. Hybrid prediction modelling of resource consumption in the 3DP process

According to the framework in Section 4, this section defines the prediction models of time, energy and material consumptions. As shown in Eqs. (1)–(3), the total time consumption of a printing process t equals the Boolean union of four operations' time consumption levels. The model is nonlinear due to the simultaneous operations during printing, including axial motion time t_{axis}, material processing time t_{mp}, unit heating time t_{uh} and material feeding time t_{mf}. Note that the time of auxiliary operation t_a equals the total time consumption t because the auxiliary system remains on-state throughout the printing process. The total energy consumption E equals the linear accumulation of energy consumed by all operations. The model includes the energy consumption levels of axial moving E_{axis}, material processing E_{mp}, unit heating E_{uh}, material feeding E_{mf} and auxiliary E_a. The total material consumption M equals the accumulative mass of material deposited on each toolpath. ρ denotes the material density. ΔV_{path} denotes the material volume per toolpath.

$$t = t_{axis} \cup t_{mp} \cup t_{uh} \cup t_{mf} \tag{1}$$

$$E = E_{axis} + E_{mp} + E_{uh} + E_{mf} + E_a \tag{2}$$

$$M = \rho \bullet \sum \Delta V_{path} \tag{3}$$

The submodels of each operation's consumption are defined in the following subsections.

5.1. Prediction modelling of time consumption

5.1.1. Time consumption of axial moving operation

The axial moving operation has two states: working and standby. The time consumption of this operation t_{axis} is the sum of the time consumed by two states:

$$t_{axis} = t^{w}_{axis} + t^{s}_{axis} \tag{4}$$

where t^{w}_{axis} denotes the working time and t^{s}_{axis} denotes the standby time. For the commonly used three-axis 3DP system, there are three types of axial motion: printing motion on the XY plane, travelling motion on the XY plane and layer-switching motion on the *Z*-axis. Fig. 5 shows the three axial motions used to calculate t^{w}_{axis}. Each motion is described as follows.

For the first layer-switching motion, the nozzle starts from A (x_1, y_1, z_1) on $Layer_1$ and then moves to B (x_2, y_2, z_2) on $Layer_2$ at a layer-switching speed of v_z, where $x_1 = x_2$, $y_1 = y_2$, $z_1 \neq z_2$. The displacement of this motion on the Z-axis is $z_2 - z_1$. The time consumption is calculated as $\frac{z_2 - z_1}{v_z}$.

For the second printing motion on $Layer_2$, the nozzle moves from B (x_2, y_2, z_2) to C (x_3, y_3, z_3), with a material feed e at a printing speed v^1_{xy}, where $z_2 = z_3$. The displacement of this motion is $\sqrt{(x_3 - x_2)^2 + (y_3 - y_2)^2}$. The time consumption is calculated as $\frac{\sqrt{(x_3 - x_2)^2 + (y_3 - y_2)^2}}{v^1_{xy}}$.

For the final travelling motion on $Layer_2$, the nozzle moves from C (x_3, y_3, z_3) to D (x_4, y_4, z_4) without material feed at a travelling speed v^2_{xy}, where $z_3 = z_4$. The displacement of this motion is $\sqrt{(x_4 - x_3)^2 + (y_4 - y_3)^2}$. The time consumption is calculated as $\frac{\sqrt{(x_4 - x_3)^2 + (y_4 - y_3)^2}}{v^2_{xy}}$.

Based on the calculation above, the working time t^{w}_{axis} is the accumulation of time consumed for all toolpaths from the first layer to the final layer:

$$t^{w}_{axis} = \sum \frac{\sqrt{\Delta X^2 + \Delta Y^2}}{v_{xy}} + \sum \frac{\Delta Z}{v_z} \tag{5}$$

where ΔX, ΔY, and ΔZ denote the distance from the present coordinate to the next coordinate on the X-, Y-, and *Z*-axes, respectively; v_{xy} denotes the printing/travelling speed of each toolpath on the XY plane; and v_z denotes the layer-switching speed on the Z-axis. The coordinate and speed values of each axial motion are extracted from G-codes.

In the standby state, the axial moving system is time- and energy-consuming without axial motion. During printing, this state is generally simultaneous with other operations, such as the preheating of the material processing and unit heating systems. Thus, the standby time t^{s}_{axis} depends on the time consumed by other operations. The standby time mathematical model is represented by the time models of other simultaneous operations according to the GP diagram.

5.1.2. Time consumption of material processing operation

The material processing operation has two states: preheating and working. The total time consumption of this operation t_{mp} is the sum of the time consumed by two states:

$$t_{mp} = t^{p}_{mp} + t^{w}_{mp} \tag{6}$$

where t^{p}_{mp} and t^{w}_{mp} denote the preheating time and working time, respectively. In the preheating state, the material processing system is heated from the present temperature T^{0}_{mp} to the target temperature T_{mp}. The preheating time t^{p}_{mp} is determined by the temperature difference ΔT_{mp} and the heating performance of the material processing system. Therefore, we assume t^{p}_{mp} as a function of ΔT_{mp}:

$$t^{p}_{mp} = f(\Delta T_{mp}) \tag{7}$$

$$\Delta T_{mp} = T_{mp} - T^{0}_{mp} \tag{8}$$

The function coefficients can be regressed based on the experimental data collected from the material processing system. In the working state, the heating remains at T_{mp} until the end of printing. This state is simultaneous with the states of other operations, such as axial moving and material feeding. Thus, according to the GP diagram, the model of working time t^{w}_{mp} is represented by the time models of other simultaneous operations.

5.1.3. Time consumption of unit heating operation

The unit heating operation has two states: preheating and working. The total time consumption of this operation t_{uh} is the sum of the time consumed by two states:

$$t_{uh} = t^{p}_{uh} + t^{w}_{uh} \tag{9}$$

where t^{p}_{uh} and t^{w}_{uh} denote the preheating time and working time, respectively. In a similar way, t^{p}_{uh} is determined by the temperature difference ΔT_{uh} and the heating performance of the unit heating system. Therefore, we assume t^{p}_{uh} as a function of ΔT_{uh}:

$$t^{p}_{uh} = f(\Delta T_{uh}) \tag{10}$$

$$\Delta T_{uh} = T_{uh} - T^{0}_{uh} \tag{11}$$

where T^{0}_{uh} and T_{uh} denotes the present temperature and target temperature, respectively. The function coefficients can be regressed based on the experimental data collected from the unit heating subsystem. In the working state, the heating remains at T_{uh}. The working time t^{w}_{uh} depends on the time of other simultaneous operations.

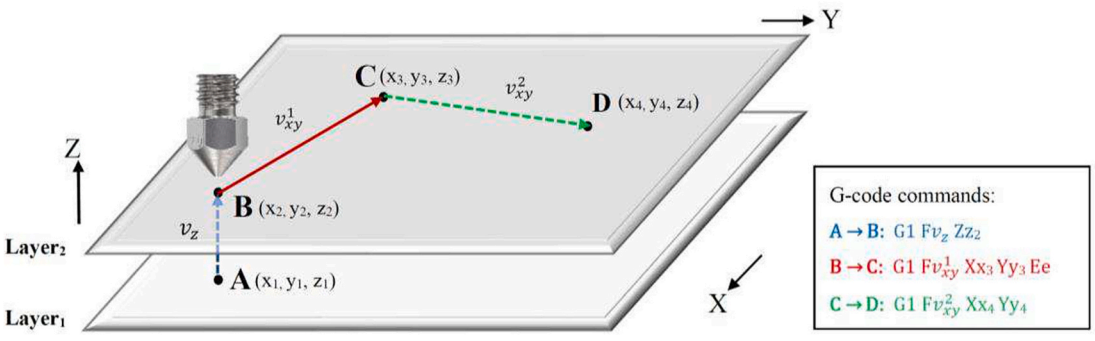

Fig. 5. Typical toolpaths for the general three-axial moving system.

5.1.4. Time consumption of material feeding operation

The material feeding operation has two states: working and standby. The time consumption of this operation t_{mf} is the sum of the time consumed by two states:

$$t_{mf} = t^{w}_{mf} + t^{s}_{mf} \tag{12}$$

where t^{w}_{mf} denotes the working time and t^{s}_{mf} denotes the standby time. For ME, DED, and PLM technologies, the operation is in the working state during the material deposition process and runs simultaneously with axial moving to extrude thermoplastic filaments or spray metal powders along the specified toolpaths. In this case, t^{w}_{mf} equals the working time of axial moving t^{w}_{axis}:

$$t^{w}_{mf} = t^{w}_{axis} \tag{13}$$

For BJ, PBF and SL technologies, the material feeding operation is driven by the powder roller or sheet roller to supply material for a new layer; simultaneously, the axial moving operation is in the standby state. In this case, t^{w}_{mf} is modelled as follows:

$$t^{w}_{mf} = t_{layer} \bullet N \tag{14}$$

where t_{layer} denotes the time for one layer's material feeding and N denotes the layer numbers, and its value is determined by the part height and layer thickness. The standby time t^{s}_{mf} depends on the times of other simultaneous operations.

5.1.5. Time consumption of auxiliary operation

The auxiliary operation is always in a working state to monitor and control printing progression. The time consumption t_a of this operation is represented by the Boolean union of other operations' time consumption levels:

$$t_a = t_{axis} \cup t_{mp} \cup t_{uh} \cup t_{mf} \tag{15}$$

5.2. Prediction modelling of energy consumption

Energy consumption is modelled as the integral of power over the runtime of each machine subsystem. The energy model is built based on the time models.

5.2.1. Energy consumption of axial moving operation

The energy of axial moving operation E_{axis} is the sum of the energy levels consumed by the working and standby states:

$$E_{axis} = \int_0^{t^{w}_{axis}} P^{w}_{axis} dt + \int_0^{t^{s}_{axis}} P^{s}_{axis} dt \tag{16}$$

where P^{s}_{axis} denotes the standby power; P^{w}_{axis} denotes the working power assumed as a function of the travelling speed v_{xy} on the XY plane and the layer-switching speed v_z on the Z-axis:

$$P^{w}_{axis} = f\left(v_{xy}, v_z\right) \tag{17}$$

5.2.2. Energy consumption of material processing operation

The energy of the material processing operation E_{mp} is the sum of the energy levels consumed by the preheating and working states:

$$E_{mp} = \int_0^{t^{p}_{mp}} P^{p}_{mp} dt + \int_0^{t^{w}_{mp}} P^{w}_{mp} dt \tag{18}$$

where P^{p}_{mp} and P^{w}_{mp} denote the preheating power and working power, respectively, and are assumed as functions of the target temperature T_{mp}:

$$P^{p}_{mp} = f\left(T_{mp}\right) \tag{19}$$

$$P^{w}_{mp} = f\left(T_{mp}\right) \tag{20}$$

5.2.3. Energy consumption of unit heating operation

The energy of unit heating operation E_{uh} is the sum of the energy levels consumed by the preheating and working states:

$$E_{uh} = \int_0^{t^{p}_{uh}} P^{p}_{uh} dt + \int_0^{t^{w}_{uh}} P^{w}_{uh} dt \tag{21}$$

where P^{p}_{uh} and P^{w}_{uh} denote the preheating power and working power, respectively, and are assumed as functions of the target temperature T_{uh}:

$$P^{p}_{uh} = f(T_{uh}) \tag{22}$$

$$P^{w}_{uh} = f(T_{uh}) \tag{23}$$

5.2.4. Energy consumption of material feeding operation

The energy of material feeding operation E_{mf} is the sum of the energy levels consumed by the working and standby states:

$$E_{mf} = \int_0^{t^{w}_{mf}} P^{w}_{mf} dt + \int_0^{t^{s}_{mf}} P^{s}_{mf} dt \tag{24}$$

where P^{s}_{mf} denotes the standby power and P^{w}_{mf} denotes the working power assumed as a function of the printing speed v_{xy}:

$$P^{w}_{mf} = f\left(v_{xy}\right) \tag{25}$$

5.2.5. Energy consumption of auxiliary operation

The auxiliary operation remains a constant power P_a during printing. The energy consumption E_a of the auxiliary operation is modelled as follows:

$$E_a = P_a \bullet t_a \tag{26}$$

5.3. Prediction modelling of material consumption

The material feed on each toolpath follows G-code commands. The total mass M of material consumption is modelled as follows:

$$M = \rho \bullet \sum \Delta V_{path} \tag{27}$$

where ρ denotes the material density and e denotes the deposited material volume on each toolpath, which is calculated according to the material properties. For example, a commonly used material for FDM is polylactic acid (PLA) filaments. In this case, ΔV_{path} represents the volume of material filament extruded on each toolpath:

$$\Delta V_{path} = \Delta \ell_{path} \pi \frac{r^2}{4} \tag{28}$$

where r and $\Delta \ell_{path}$ denote the cross-sectional diameter and the extruded length of the thermoplastic filament, respectively. $\Delta \ell_{path}$ can be obtained through physical modelling based on G-codes. For example, in a command line "G1 F600 X17.156 Y26.687 E1.265", the command "E1.265" indicates that the accumulative length of deposited material is 1.265 mm, thus $\sum \Delta \ell_{path} = 1.265$.

5.4. Summary of time and power for resource consumption model assembly

The submodels of time and power defined in the previous sections are used to assemble the final consumption models of time and energy, as shown in Fig. 6. It can be seen that there are four types of parameters to be modelled: parameters calculated from G-codes, parameters modelled based on GP diagram, independent parameters and dependent parameters modelled through experiments.

Regarding time consumption, the submodels of preheating time for material processing t^{p}_{mp} and unit heating t^{p}_{uh} are obtained through data-

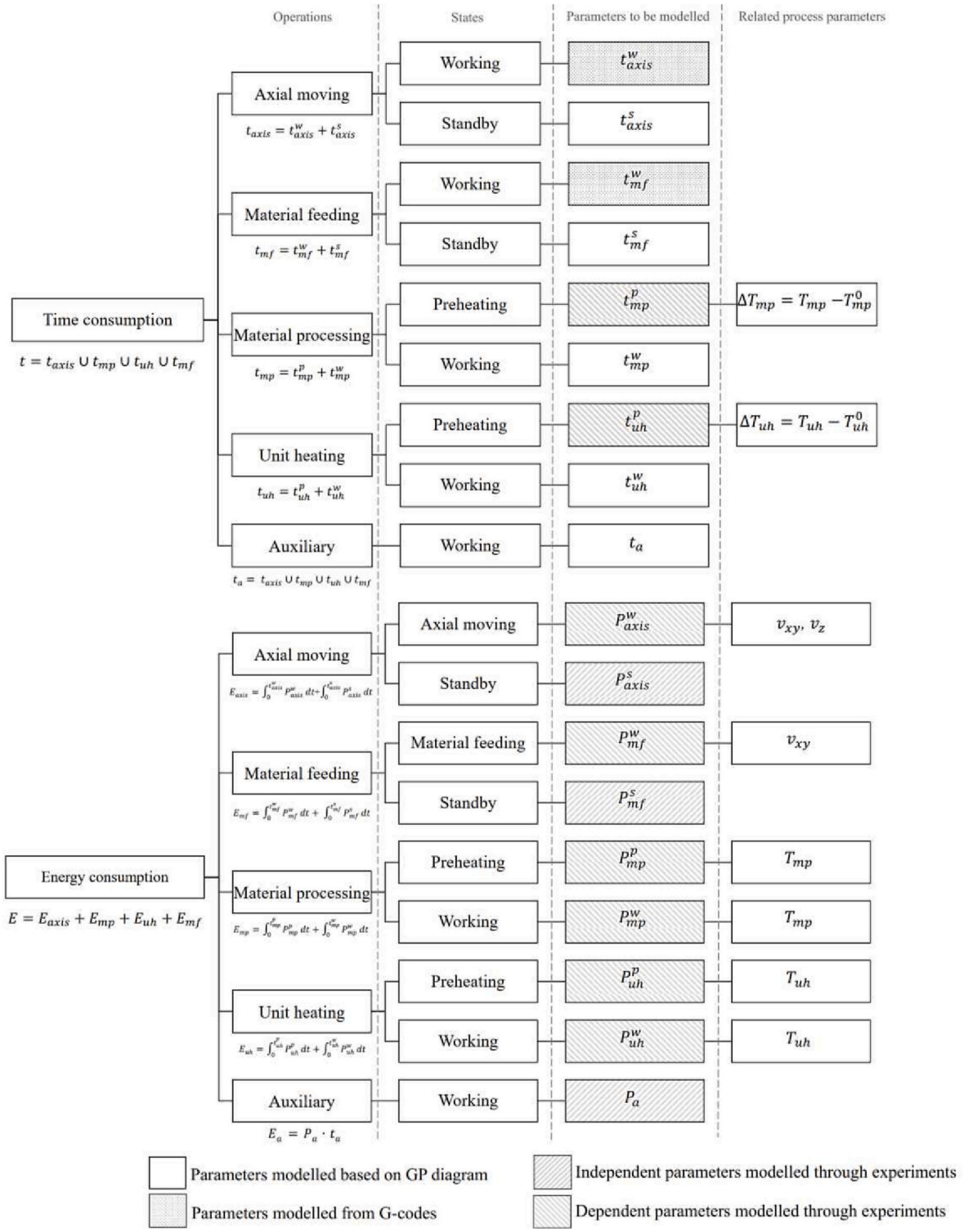

Fig. 6. Tree diagrams of parameters for assembling time and energy consumption models.

driven modelling. During experiments, t^p_{mp} and t^p_{uh} are measured under different temperature differences ΔT_{mp} and ΔT_{uh}, respectively. Experimental data are collected to regress the mathematical models of t^p_{mp} and t^p_{uh}. For the axial moving and material feeding operations, the working times t^w_{axis} and t^w_{mf} are modelled physically based on G-codes. With the assist of GP diagram, other time consumptions t^s_{axis}, t^s_{mf}, t^w_{mp}, t^w_{uh} and t_a are modelled based on t^p_{mp}, t^p_{uh}, t^w_{axis} and t^w_{mf} due to their simultaneous operations during printing.

Regarding energy consumption, the submodels of powers in different operation states are obtained through data-driven modelling. The dependent parameters P^w_{axis}, P^w_{mf}, P^p_{mp}, P^w_{mp}, P^p_{uh}, P^w_{uh} are measured at different values of related process parameters. Then, the mathematical model of each power is derived from experimental data by using a regression tool. The independent parameters P^w_{axis} and P_a are measured as constants.

6. Hybrid prediction modelling for real-world 3DP machines

The hybrid prediction modelling method proposed in the previous sections is applied to two real 3DP machines. First, the hardware and software environments are assembled to support the modelling. The generation of the GP diagram and the identification of operation states are presented. Then, the methods of G-code calculation for physical modelling and experimental measurements for data-driven modelling are described. After the preparation work, the consumption modelling for each machine is demonstrated. The details of the modelling process are as follows.

6.1. Hardware and software environment

For the hardware, two FDM machines, Anycubic i3 Mega FDM 3D printer and Monoprice MP Mini Delta FDM printer, are used as test cases in the ME category. The raw material is a 1.75-mm-diameter PLA filament, which is deposited through wire extrusion. The power meter is a Yokogawa CW500 power quality analyser, which is used to record the times and powers of machine subsystems. The circuit connection of the CW500 and FDM machine is shown in Fig. 7. For the software, SolidWorks and Cura are used at the CAD and CAM stages. The polynomial regression tool used in data-driven modelling is provided by MATLAB.

Fig. 8 presents the consumption-related machine units of two machines, which are classified into five subsystems, as listed in Table 3. The machine specifications are listed in Table 4. For both machines, the material feeding system is a wire extruder driven by a stepper motor to load PLA filaments. The material processing system is the nozzle hotend used to melt the filament. The unit heating system is the build platform, which is heated to fix the platform workpiece base. The auxiliary system includes temperature sensors, a display unit, cooling fans, a user interface and connectivity tools, which are used to monitor and control the printing progression.

The difference between the two machines is the axial moving system. The Anycubic machine uses the Cartesian system consisting of three independent stepper motors. Each motor drives nozzle motion on one axis. The Monoprice machine uses a Delta system consisting of three parallel stepper motors. The axial motion is driven through the linkage motion of three stepper motors.

6.2. Generation of GP diagram and identification of operation states

To understand the workflow of machine operations, a GP diagram is generated by three steps, as demonstrated in Fig. 9.

- First, the machine is assigned to print a random geometry using default process parameters. The power profile of the printing process is captured by CW500.

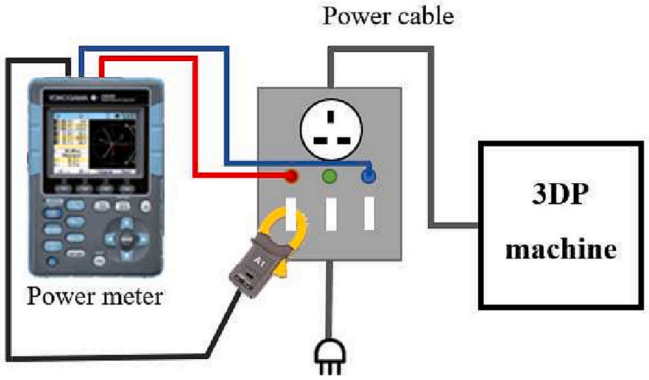

Fig. 7. Circuit connection of the 3DP machine and power meter.

- Second, using the same process parameters, the power profiles of the independently running subsystems are captured.
- Finally, the obtained power profiles are integrated to formulate the GP diagram, where the starting time of each operation corresponds to its G-code command and the step change in the power profile.

In the GP diagram, the operation states are identified based on G-codes. For example, the unit heating operation begins first by following the command "M190". When reaching the target temperature, the material processing operation starts by following the command "M109". Meanwhile, the unit heating operation switches to the working state and maintain the target temperature. For unit heating, the period from "M190" to "M109" denotes the preheating state, and the period from "M109" to the end of printing denotes the working state.

6.3. Implementation of the hybrid prediction modelling method for real-world 3DP machines

The hybrid prediction modelling method is implemented on the Anycubic and Monoprice machines. The calculation of G-codes for physical modelling and the experimental measurements for data-driven modelling are demonstrated.

6.3.1. G-code calculation for physical modelling

G-codes are used to predict the working time of axial moving operation t^{w}_{axis} and material feed $\Delta\ell_{path}$ per toolpath. To automate the G-code calculations, the corresponding computing program is compiled by using Python 3.10. The workflow is shown in Fig. 10. For a newly generated G-code file, the commands are read from the first line. When meeting a command starting with "G1" or "G0", the coordinates, speeds and material feeds are extracted and used to calculate $\frac{\sqrt{\Delta X^2+\Delta Y^2}}{v_{xy}}$, $\frac{\Delta Z}{v_z}$ and ΔV_{path}. Then, the calculation continues to the next command line until all lines are read (i.e., $k = C_N$, where C_N denotes the total number of command lines). The working time t^{w}_{axis} is the accumulation of time consumed for all motions. The material consumption M is the accumulation of material feed for all toolpaths.

6.3.2. Experimental measurements for data-driven modelling

Regarding the experimental measurements for data-driven modelling, the parameters to be measured are listed in Table 5. According to [29], the recommended sample size for a polynomial regression is at least 25. In this study, experiments are designed to measure each parameter under 25 different values of related process parameter.

For FDM technology, the axial moving and material feeding work simultaneously to deposit the melted PLA on specified toolpaths. In this case, the powers of two operations are measured simultaneously. First, a G-code file is created, in which three types of G-code commands are manually programmed. "G1 Fv_{xy} X Y" commands axial moving on the XY plane at a travelling speed v_{xy}. "G1 Fv_{xy} X Y E" commands axial moving with material feed on the XY plane at a printing speed v_{xy}. "G1 Fv_z Z" commands axial moving on the Z-axis at a layer-switching speed v_z. The coordinate values are set within the build space of the FDM machine. The values of v_{xy} are set within the boundary from the minimum v^{min}_{xy} to the maximum travelling/printing speeds v^{max}_{xy}. The values of v_z are set within the boundary from the minimum v^{min}_{z} to the maximum layer-switching speeds v^{max}_{z}. During experiments, the axial moving and material feeding systems are activated to execute predefined commands, meanwhile, their working power $P^{w}_{axis} + P^{w}_{mf}$ is measured by CW500. When all motions are complete, the two operations switch to the standby state, meanwhile, their standby power $P^{s}_{axis} + P^{s}_{mf}$ is measured.

To drive the unit heating operation, "M190 ST_{uh}" is manually programmed. The values of the target temperature T_{uh} are set within the boundary from room temperature T_0 to the maximum temperature T^{max}_{uh} of the unit heating system. Then, the values of temperature difference Δ

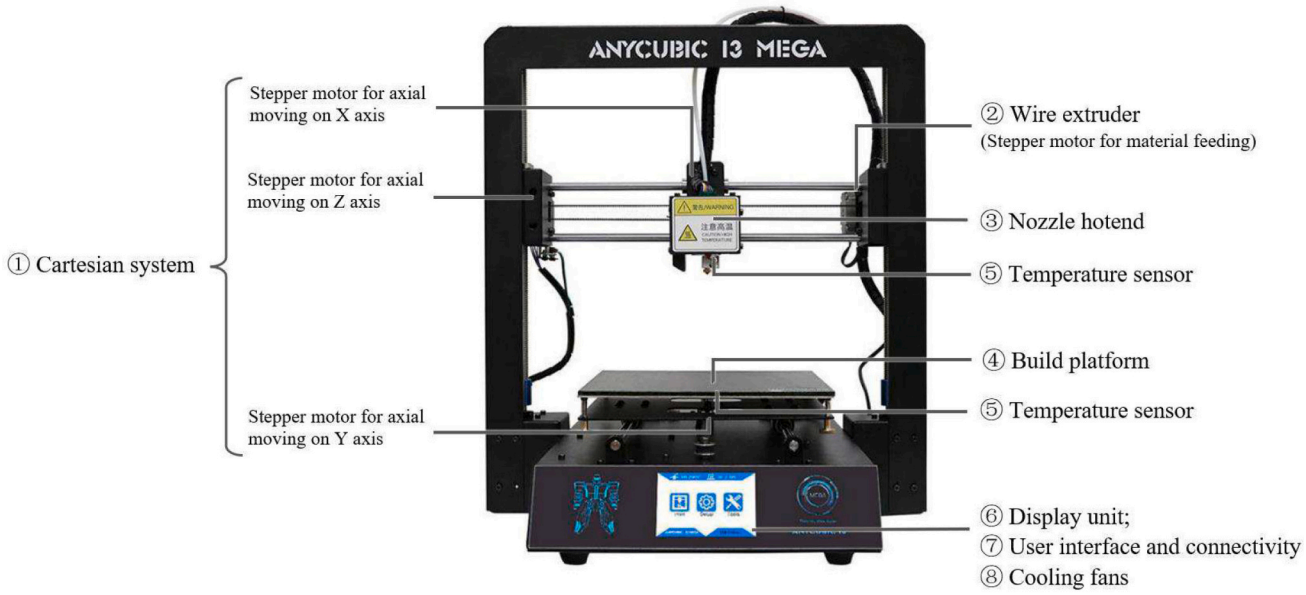

(a) Anycubic i3 Mega FDM 3D printer

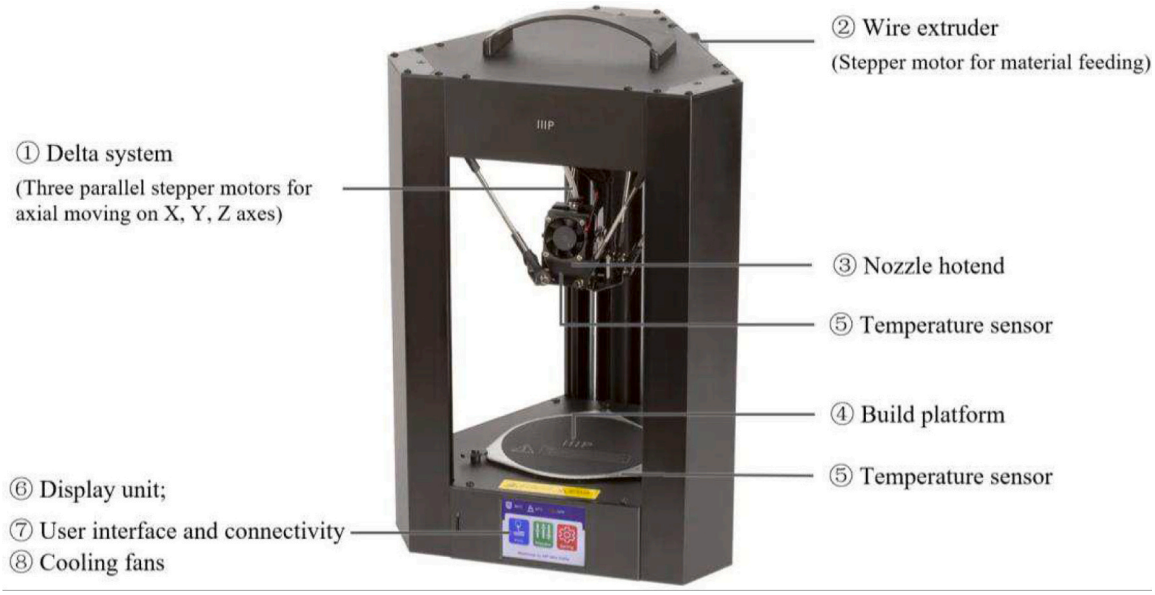

(b) Monoprice MP Mini Delta FDM 3D printer

Fig. 8. Consumption-related machine units of two FDM machines [33,34].

Table 3
Classification of machine units for the Anycubic and Monoprice machines.

3DP subsystems	Anycubic	Monoprice
Axial moving	① Cartesian system	① Delta system
Material feeding	② Wire extruder	② Wire extruder
Material processing	③ Nozzle hotend	③ Nozzle hotend
Unit heating	④ Build platform	④ Build platform
Auxiliary	⑤ Temperature sensors	⑤ Temperature sensors
	⑥ Display unit	⑥ Display unit
	⑦ User interface and connectivity	⑦ User interface and connectivity
	⑧ Cooling fans	⑧ Cooling fans

Table 4
Specifications for the Anycubic and Monoprice machines.

	Anycubic	Monoprice
Layer thickness	0.04–0.3 *mm*	0.05–0.2 *mm*
Infill density	0–100 %	0–100 %
Maximum material processing temperature	250 °C	260 °C
Maximum unit heating temperature	80°C	60°C
PLA melting point	180 °C	180 °C
Filament diameter	1.75 *mm*	1.75 *mm*
Printing speed	10–150 *mm/s*	10–150 *mm/s*
Travelling speed	10–300 *mm/s*	10–150 *mm/s*
Layer-switching speed	5 *mm/s*	10–150 *mm/s*

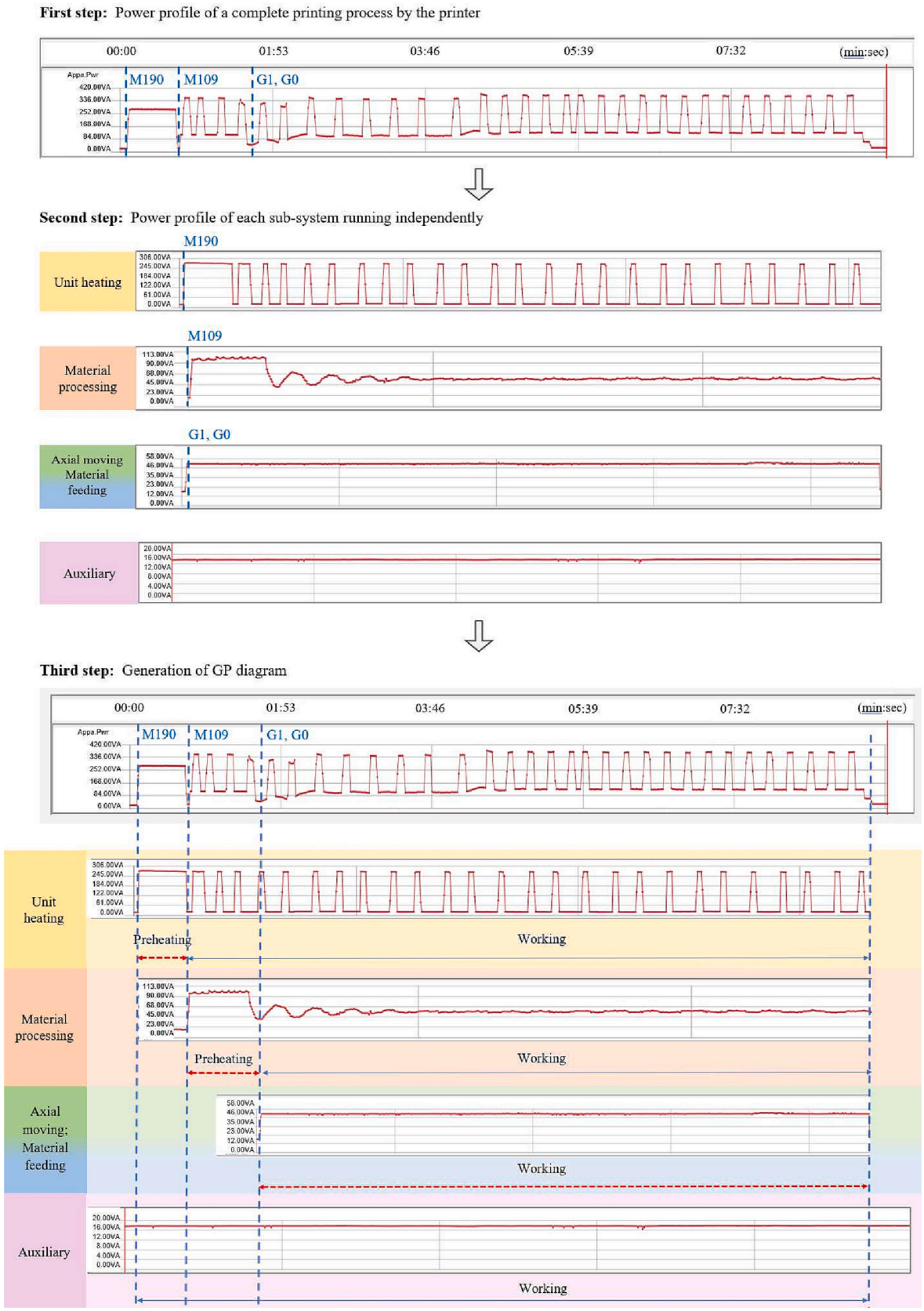

Fig. 9. Generation of GP diagram for the Anycubic machine.

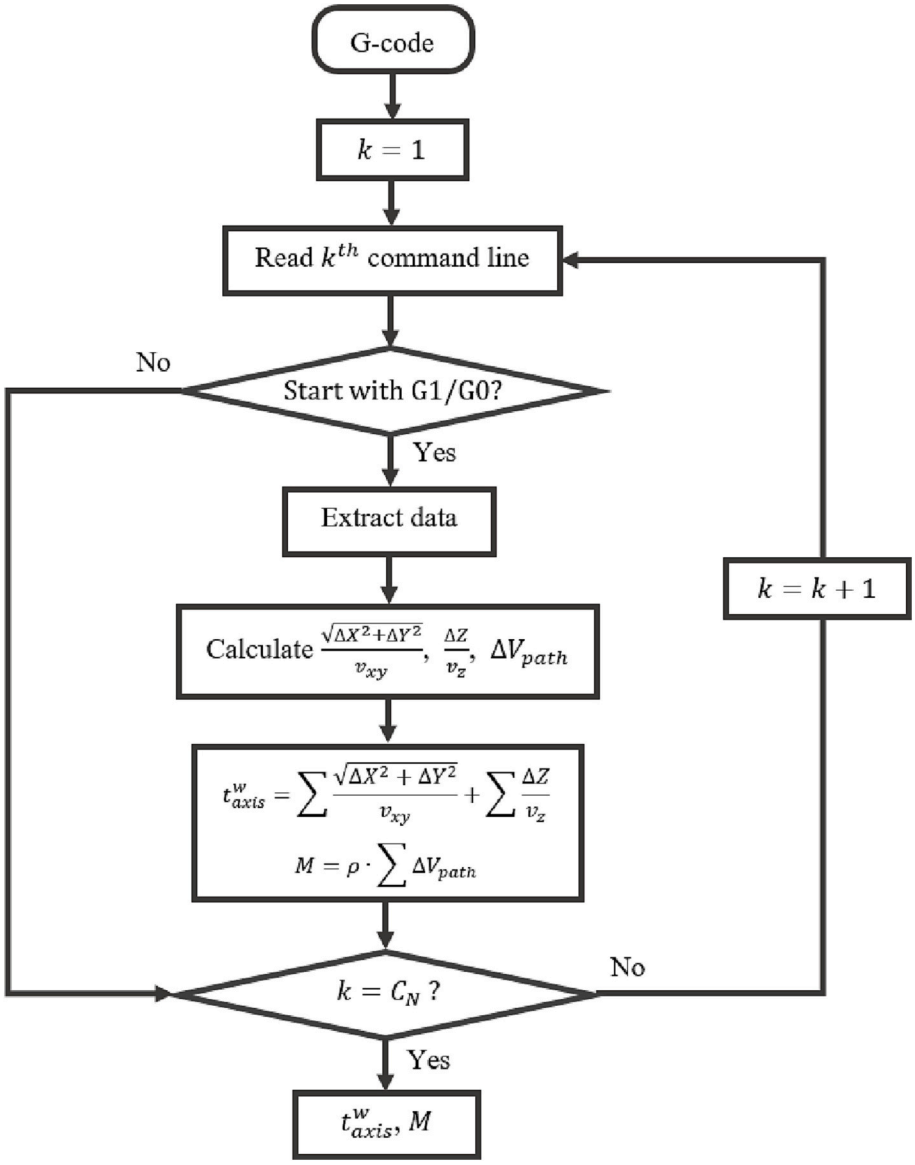

Fig. 10. Computational workflow of the G-code calculation.

Table 5
Experimental measurements for data-driven modelling.

Operations	State	Parameters	Related process parameter	Boundaries of process parameters	G-code commands
Axial moving and material feeding	Working	$P^w_{axis} + P^w_{mf}$	v_{xy},v_Z	$v_{xy} \in \left[v^{min}_{xy}, v^{max}_{xy}\right]$ $v_z \in \left[v^{min}_z, v^{max}_z\right]$	G1 Fv_{xy} X Y G1 Fv_{xy} X Y E G1 Fv_z Z
	Standby	$P^s_{axis} + P^s_{mf}$	None		
Unit heating	Preheating	t^p_{uh}	ΔT_{uh}	$T_{uh} \in [T_0, T^{max}_{uh}]$ $\Delta T_{uh} \in [0, T_{uh} - T_0]$	M190 ST_{uh}
		P^p_{uh}	T_{uh}		
	Working	P^w_{uh}	T_{uh}		
Material processing	Preheating	t^p_{mp}	ΔT_{mp}	$T_{mp} \in \left[T_0, T^{max}_{mp}\right]$ $\Delta T_{uh} \in \left[0, T_{mp} - T_0\right]$	M109 ST_{mp}
		P^p_{mp}	T_{mp}		
	Working	P^w_{mp}	T_{mp}		
Auxiliary	Working	P_a	None		

T_{uh} are set within the boundary from zero to $T_{uh} - T_0$. The present temperature of the system T^o_{uh} equals $T_{uh} - \Delta T_{uh}$. During experiments, the system is preheated for a temperature difference ΔT_{uh} from T^o_{uh} to T_{uh}, and then remains at the target temperature T_{uh}. The preheating time t^p_{uh}, preheating power P^p_{uh} and working power P^w_{uh} are measured by CW500.

To drive the material processing operation, "M109 ST_{mp}" is programmed. The values of the target temperature T_{mp} are set within the boundary from room temperature T_0 to the maximum temperature T^{max}_{mp} of the material processing system. The values of ΔT_{uh} are set within the

boundary from zero to $T_{mp} - T_0$. The present temperature T^o_{mp} is $T_{mp} - \Delta T_{mp}$. During experiments, the system preheats from T^0_{mp} to T_{mp} and remains at T_{mp}. The preheating time t^p_{mp}, preheating power P^p_{mp} and working power P^w_{mp} are measured.

The auxiliary operation begins when the machine is booted. The working power P_a is measured at the machine idle state.

6.4. Predictive models of the Anycubic i3 Mega FDM printer

The consumption models for the Anycubic machine are developed in this section. First, the GP diagram for the machine is generated by following the method in Section 6.2 and shown in Fig. 11.

6.4.1. Predictive models of time consumption

The time consumption t is the Boolean union of time consumed for five operations. According to Fig. 11, t is the sum of the preheating time for material processing t^p_{mp}, preheating time for unit heating t^p_{uh} and working time for axial moving t^w_{axis}:

$$t = t^p_{uh} + t^p_{mp} + t^w_{axis} \tag{29}$$

where t^p_{uh} and t^p_{mp} are functions related to ΔT_{uh} and ΔT_{mp}, respectively. By following the experimental measurement method in Section 6.3.2, the regression models of t^p_{uh} and t^p_{mp} are shown in Table 6. The regression curve of t^p_{mp}, for example, is shown in Fig. 12, where $\Delta T_{mp} \in [49, 198]$ and the goodness of fit $R^2 = 0.9975$. In the working state, the working time of unit heating t^w_{uh} overlaps t^p_{mp} and t^w_{axis} (see Fig. 11); thus, $t^w_{uh} = t^p_{mp} + t^w_{axis}$. The working time of material processing t^p_{mp} overlaps t^w_{axis}; thus, $t^w_{mp} = t^w_{axis}$.

Table 6
Time consumption models for the Anycubic machine.

Total time consumption		$t = t^p_{uh} + t^p_{mp} + t^w_{axis}$	
Operations	States	Predictive models	Regression results
Axial moving t_{axis}	Working	$t^w_{axis} = \sum \frac{\sqrt{\Delta X^2 + \Delta Y^2}}{v_{xy}} + \sum \frac{\Delta Z}{v_z}$	
Material feeding t_{mf}	Working	$t^w_{mf} = t^w_{axis}$	
Material processing t_{mp}	Preheating	t^p_{mp}=0.000515$\Delta T_{mp}{}^2$ + 0.2395ΔT_{mp} + 11.7	Appendix A.1
	Working	$t^w_{mp} = t^w_{axis}$	
Unit heating t_{uh}	Preheating	t^p_{uh} = 0.05759$\Delta T_{uh}{}^2$ + 2.98ΔT_{uh} − 2.098	Appendix A.2
	Working	$t^w_{uh} = t^p_{mp} + t^w_{axis}$	
Auxiliary t_a	Working	$t_a = t$	

In this case, the axial moving operation begins after the machine unit preheating. In the material deposition process, the axial moving operation remains in the working state without standby (i.e., $t^s_{axis} = 0$). By following the method of G-code calculation in Section 6.3.1, the working time t^w_{axis} is calculated from G-codes. The material feeding operation remains in the working state and is simultaneous with axial moving without standby (i.e., $t^m_{mf} = t^w_{axis}$, $t^s_{mf} = 0$). The auxiliary time t_a equals

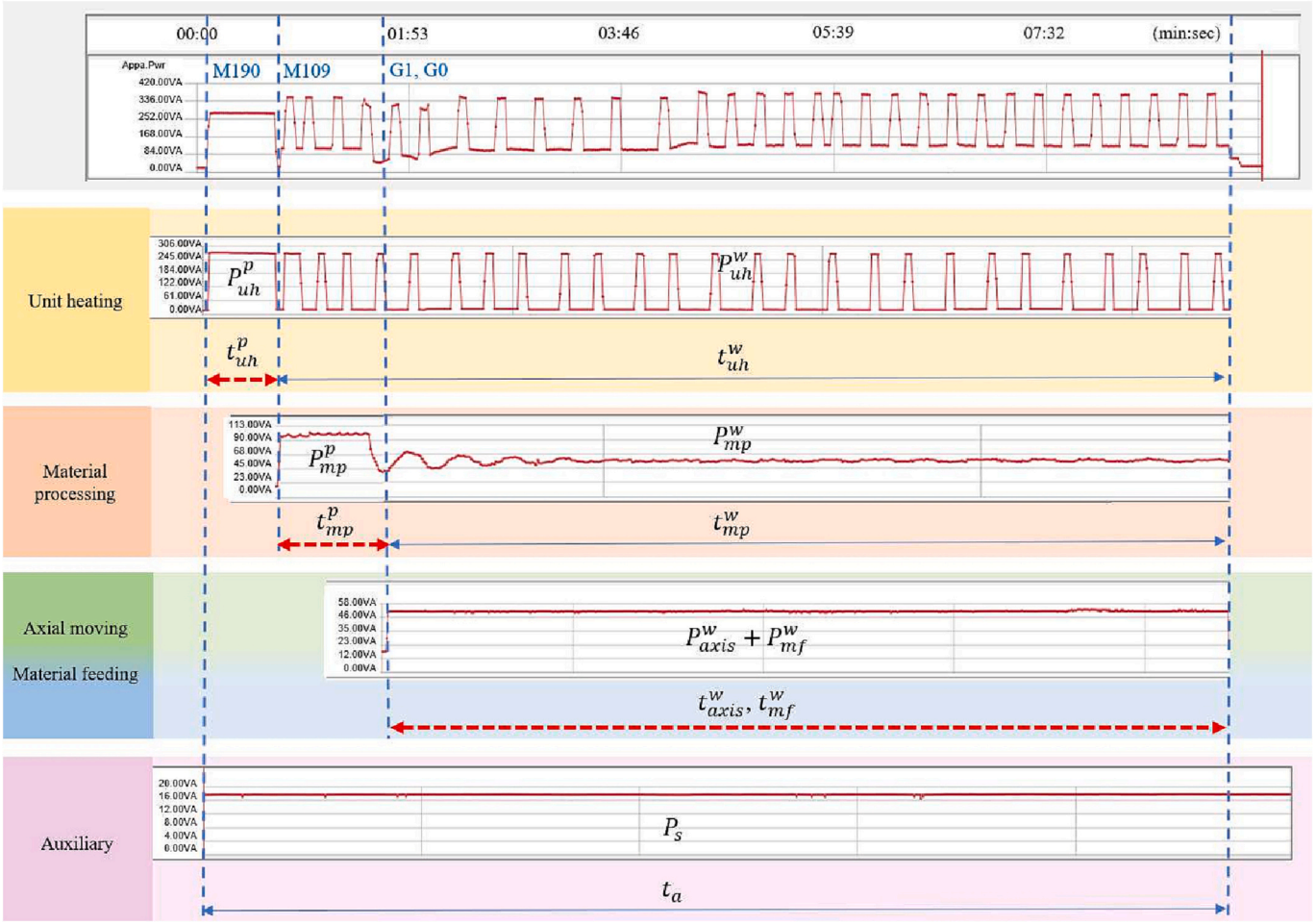

Fig. 11. GP diagram for the Anycubic machine.

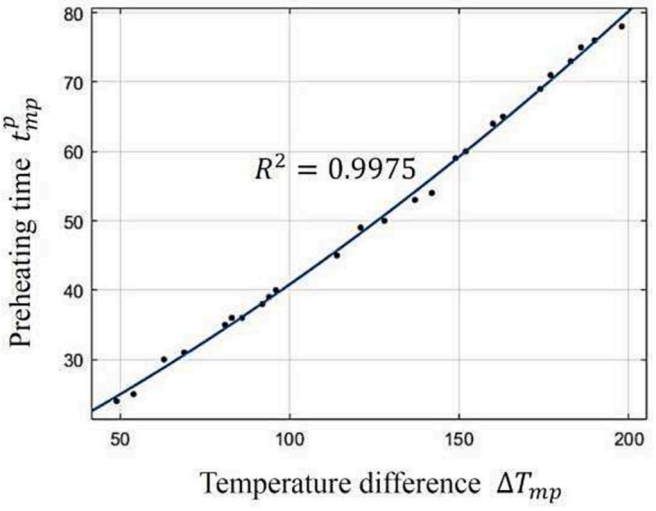

Fig. 12. Regression curve for preheating time t^p_{mp}.

the total time consumption (i.e., $t_a = t$). Table 6 shows a summary of the time consumption modelling results.

6.4.2. Predictive models of energy consumption

In terms of energy models, the preheating power of material processing P^p_{mp} remains at 85.73614 VA. The working power P^w_{mp} is gradually stabilised to a constant, and its value is functionally related to the target temperature T_{mp}. The preheating power P^p_{uh} of unit heating remains at 307.96224 VA. The average working power P^w_{uh} is functionally related to the target temperature T_{uh}. The working powers of material feeding and axial moving $P^w_{axis} + P^w_{mf}$ remain at 42.47047 VA. The auxiliary power P_a remains at 28.06063 VA. Table 7 shows a summary of the energy consumption modelling results.

6.4.3. Predictive models of material consumption

Table 8 presents the material consumption model. By following the physical modelling method in Section 6.3.1, the extruded length of PLA filament per toolpath $\Delta\ell_{path}$ is extracted from G-codes.

6.5. Predictive models of the Monoprice MP Mini Delta FDM printer

The GP diagram of the Monoprice machine is shown in Fig. 13. In this case, there is a preparatory phase before the printing to zero the material feed, then calibrate and return the nozzle position to home. Thus, the

Table 7
Energy consumption models of five operations for the Anycubic machine.

Total energy consumption		$E = E_{axis} + E_{mp} + E_{uh} + E_{mf} + E_a$	
Operations	States	Predictive models	Regression results
Axial moving and material feeding $E_{axis} + E_{mf}$	Working	$P^w_{axis} + P^w_{mf} = 42.47047(VA)$ Energy consumption: $E_{axis} + E_{mf} = \left(P^w_{axis} + P^w_{mf}\right) t^w_{axis}$	
Material processing E_{mp}	Preheating	$P^p_{mp} = 85.73614(VA)$	Appendix A.1
	Working	$P^w_{mp} = -0.0002833{T_{mp}}^2 + 0.3428T_{mp} - 13.44$ Energy consumption: $E_{mp} = P^p_{mp} t^p_{mp} + P^w_{mp} t^w_{mp}$	
Unit heating E_{uh}	Preheating	$P^p_{uh} = 307.96224(VA)$	Appendix A.2
	Working	$P^w_{uh} = 2.252T_{uh} - 48.64$ Energy consumption: $E_{uh} = P^p_{uh} t^p_{uh} + P^w_{uh} t^w_{uh}$	
Auxiliary E_a	Working	$P_a = 28.06063(VA)$ Energy consumption: $E_a = P_a \bullet t_a$	

Table 8
Material consumption models for the Anycubic machine.

Total material consumption		$M = \rho \bullet \sum \Delta V_{path}$
Operation	States	Predictive models
Material feeding	Working	$\rho = 1.24g/cm^3$ $r = 1.75mm$ $\Delta V_{path} = \Delta\ell_{path}\pi\frac{r^2}{4}$

axial moving and material feeding systems are activated from the beginning of the printing process. Since the last nozzle coordinate and material feed in the previous 3DP task are unknown, the resource consumption in the preparatory phase is not considered in this case.

6.5.1. Predictive models of time consumption

According to Fig. 13, the time consumption t is the sum of the preheating time of material processing t^p_{mp} and the working time of axial moving t^w_{axis}:

$$t = t^p_{mp} + t^w_{axis} \tag{30}$$

In this case, due to the built-in algorithm of Cura for this machine, the material processing operation is commanded to preheat the nozzle hotend to a temperature 5 °C higher than the target temperature (i.e., $T_{mp} + 5$). In the working state, the operation remains at the temperature $T_{mp} + 5$ during the printing of the first layer. When the first layer is printed, the temperature decreases to T_{mp}. Thus, the material processing time is the sum of time consumed by the three parts:

$$t_{mp} = t^p_{mp} + t^{w_1}_{mp} + t^{w_2}_{mp} \tag{31}$$

where the preheating time t^p_{mp} is functionally related to ΔT_{mp} and $t^{w_1}_{mp}$ denotes the working time at temperature $T_{mp} + 5$, which overlaps the axial moving time for the first layer $\sum \frac{\Delta l^1_{xy}}{v^1_{xy}}$; thus, $t^{w_1}_{mp} = \sum \frac{\Delta l^1_{xy}}{v^1_{xy}}$. The value of $\sum \frac{\Delta l^1_{xy}}{v^1_{xy}}$ is calculated from G-codes. $t^{w_2}_{mp}$ denotes the working time at temperature T_{mp}, which overlaps the axial moving time for the remaining layers; thus, $t^{w_2}_{mp} = t^w_{axis} - t^{w_1}_{mp}$.

The unit heating starts from the completion of the first layer. The preheating time t^w_{uh} is functionally related to the temperature difference ΔT_{uh}. The working time t^w_{uh} overlaps $t^{w_2}_{mp}$ excluding t^p_{uh}; thus, $t^w_{uh} = t^{w_2}_{mp} - t^p_{uh}$.

The axial moving operation has two states: standby and working. The standby time t^s_{axis} overlaps t^p_{mp}; thus, $t^s_{axis} = t^p_{mp}$. The working time t^w_{axis} is calculated from G-codes.

The material feeding operation is simultaneous with axial moving, which has two states: standby and working. The standby time t^s_{mf} overlaps t^p_{mp}; thus, $t^s_{mf} = t^p_{mp}$. The working time overlaps t^w_{axis}; thus, $t^w_{mf} = t^w_{axis}$.

The auxiliary time t_a equals the total time consumption (i.e., $t_a = t$). Table 9 shows a summary of the time consumption modelling results.

6.5.2. Predictive models of energy consumption

In energy models, the preheating power of material processing P^p_{mp} remains at 61.12736 VA. The working power P^w_{mp} is functionally related to the target temperature T_{mp}. In this case, since the system is heated to temperature $T_{mp} + 5$ until the completion of the first layer, the total energy consumption is the sum of three parts: 1) $P^p_{mp} t^p_{mp}$ is the energy consumed in the preheating state at temperature $T_{mp} + 5$; 2) $P^{w_1}_{mp} t^{w_1}_{mp}$ is the energy consumed in the working state at temperature $T_{mp} + 5$; 3) $P^{w_2}_{mp} t^{w_2}_{mp}$ is the energy consumed in the working state at target temperature T_{mp}.

The preheating power P^p_{uh} and working power P^w_{uh} of unit heating are functionally related to the target temperature T_{uh}. The working power

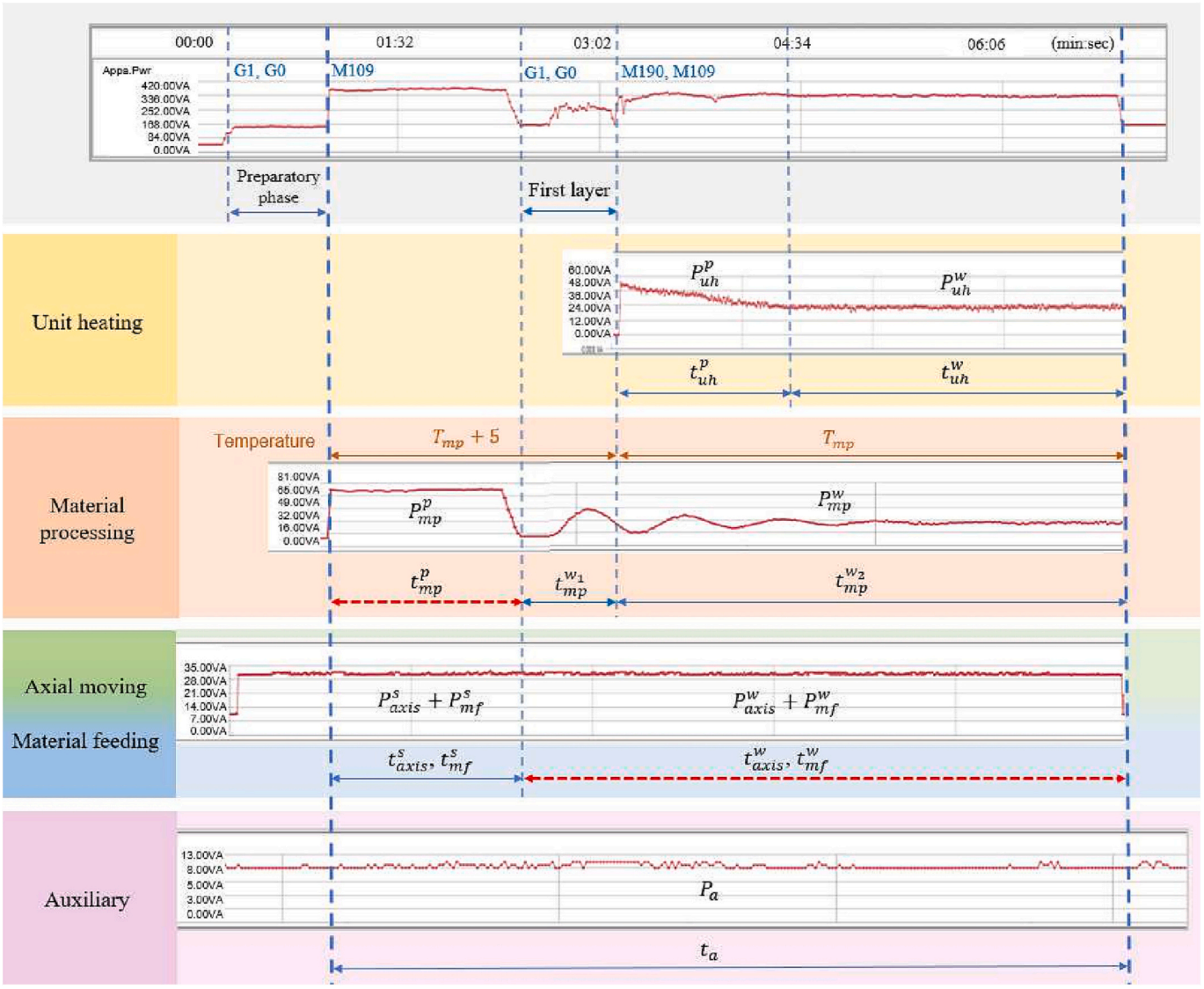

Fig. 13. GP diagram for the Monoprice machine.

Table 9
Time consumption models for the Monoprice machine.

Total time consumption		$t = t_{mp}^{p} + t_{axis}^{w}$	
Operations	States	Predictive models	Regression results
Axial moving t_{axis}	Working	$t_{axis}^{w} = \sum \frac{\sqrt{\Delta X^2 + \Delta Y^2}}{v_{xy}} + \sum \frac{\Delta Z}{v_z}$	
	Standby	$t_{axis}^{s} = t_{mp}^{p}$	
Material processing t_{mp}	Preheating	$t_{mp}^{p} = 0.0007332(\Delta T_{mp}+5)^2 + 0.2994(\Delta T_{mp}+5) + 14.31$	Appendix B.1
	Working	$t_{mp}^{w_1} = \sum \frac{\sqrt{\Delta X_1{}^2 + \Delta Y_1{}^2}}{v_{xy}^{1}}$	
		$t_{mp}^{w_2} = t_{axis}^{w} - t_{mp}^{w_1}$	
Unit heating t_{uh}	Preheating	$t_{uh}^{p} = -0.06427\Delta T_{uh}{}^2 + 6.832\Delta T_{uh} + 58.1$	Appendix B.2
	Working	$t_{uh}^{w} = t_{mp}^{w_2} - t_{uh}^{p}$	
Material feeding t_{mf}	Working	$t_{mf}^{w} = t_{axis}^{w}$	
	Standby	$t_{mf}^{s} = t_{mp}^{p}$	
Auxiliary t_a	Working	$t_a = t$	

$P_{axis}^{w} + P_{mf}^{w}$ and standby power $P_{axis}^{s} + P_{mf}^{s}$ of material feeding and axial moving remain at 28.25414 VA. The auxiliary power P_a remains at 14.34479 VA.

Table 10 shows a summary of the energy consumption modelling results.

6.5.3. Predictive models of material consumption

In this study, two FDM machines use the same PLA filament. Thus, the material consumption model is the same as the model in Table 8.

7. Experimental validations

We validate the prediction accuracies of the consumption models defined in Section 6. The experimental methodology and case studies are presented in the following subsections.

7.1. Methodology of experimental validations

The workflow of experimental validation is demonstrated in Fig. 14, which includes two parts: consumption prediction and measurement. Regarding the consumption prediction, there are three inputs into the predictive models: G-code data, present temperatures and process

Table 10
Energy consumption models for the Monoprice machine.

Total energy consumption		$E = E_{axis} + E_{mp} + E_{uh} + E_{mf} + E_a$	
Operations	States	Predictive models	Regression results
Axial moving; and material feeding $E_{axis} + E_{mf}$	Working	$P^w_{axis} + P^w_{mf} = 28.25414(VA)$	
	Standby	$P^s_{axis} + P^s_{mf} = 28.25414(VA)$	
	Energy consumption: $E_{axis} + E_{mf} = \left(P^w_{axis} + P^w_{mf}\right)\left(t^s_{axis} + t^w_{axis}\right)$		
Material processing E_{mp}	Preheating	$P^p_{mp} = 61.12736(\text{VA})$	Appendix B.1
	Working	$P^w_{mp} = 0.1369T_{mp} - 5.599$	
		$P^{w_1}_{mp} = 0.1369(T_{mp} + 5) - 5.599$	
	Energy consumption: $E_{mp} = P^p_{mp}t^p_{mp} + P^{w_1}_{mp}t^{w_1}_{mp} + P^w_{mp}t^{w_2}_{mp}$		
Unit heating E_{uh}	Preheating	$P^p_{uh} = 0.6203T_{uh} - 1.402$	Appendix B.2
	Working	$P^w_{uh} = 0.005856{T_{uh}}^2 - 0.02571T_{uh} + 6.41$	
	Energy consumption: $E_{uh} = P^p_{uh}t^p_{uh} + P^w_{uh}t^w_{uh}$		
Auxiliary E_a	Working	$P_a = 14.34479(VA)$	
	Energy consumption: $E_a = P_a \bullet t_a$		

parameters. The outputs are the predicted consumption levels. Each input is introduced as follows:

G-code data: In Cura, five major process parameters (as listed in Table 11) are randomly set within their boundaries according to the machine specifications. Other process parameters are defaults. Then, the file of G-codes is generated, from which the data of toolpaths and printing speeds are extracted and input into the time and energy models. The material feed data are input into the material consumption model.

Present temperatures: At the beginning of the printing process, the present temperatures of unit heating and material processing systems are recorded from the machine display unit and input into the time and energy models.

Process parameters: The five process parameters in Table 11 are functionally related to the preheating time and system powers. Thus, the values of those parameters must be input into the time and energy models.

By inputting the above three into the predictive models, the resource consumption is predicted. To validate the prediction accuracy, the present printing task is printed by the machine. The actual resource consumption measured by the power meter is finally compared to the predicted consumption to calculate the prediction accuracy.

7.2. Case studies

By following the experimental methodology in Section 7.1, each machine is assigned two printing tasks. The prediction and actual results of each task are presented, and the prediction accuracies are calculated.

7.2.1. Resource consumption model accuracy of the Anycubic machine

The three-view drawings of the two parts printed by the Anycubic machine are presented in Fig. 15. The values of the input parameters are listed in Table 12. The prediction and actual results are listed in Tables 13 and 14.

7.2.2. Resource consumption model accuracy of the Monoprice machine

Three-view drawings of the two parts printed by the Monoprice machine are presented in Fig. 16. To compare the accuracies of the predictive models of the two machines, Task III uses the same part geometry as Task I. The values of the input parameters are listed in Table 15. The results are listed in Tables 16 and 17.

Table 11
Five major process parameters used for validating the prediction accuracy.

Process parameters	Notations	Boundaries	Units
Target temperature of unit heating	T_{uh}	$T_{uh} \in [T_0, T^{max}_{uh}]$	°C
Target temperature of material processing	T_{mp}	$T_{mp} \in [T_0, T^{max}_{mp}]$	°C
Travelling speed	v_{xy}	$v_{xy} \in [v^{min}_{xy}, v^{max}_{xy}]$	mm/s
Printing speed	v_{xy}	$v_{xy} \in [v^{min}_{xy}, v^{max}_{xy}]$	mm/s
Layer-switching speed	v_z	$v_z \in [v^{min}_z, v^{max}_z]$	mm/s

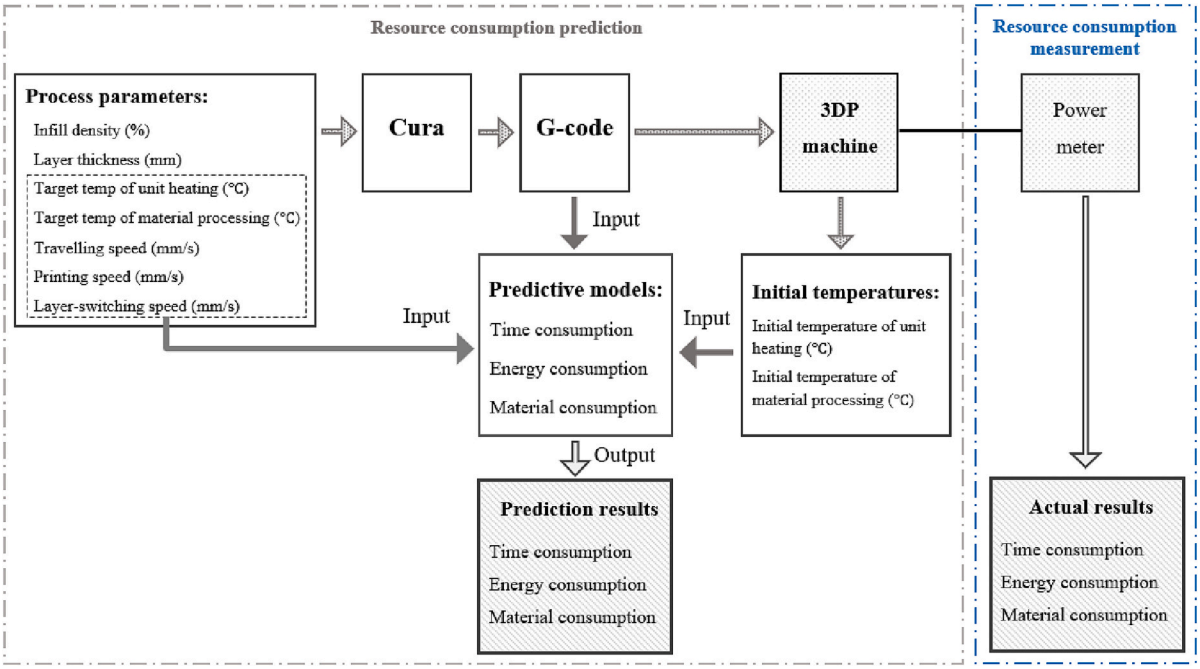

Fig. 14. Workflow of experimental validation.

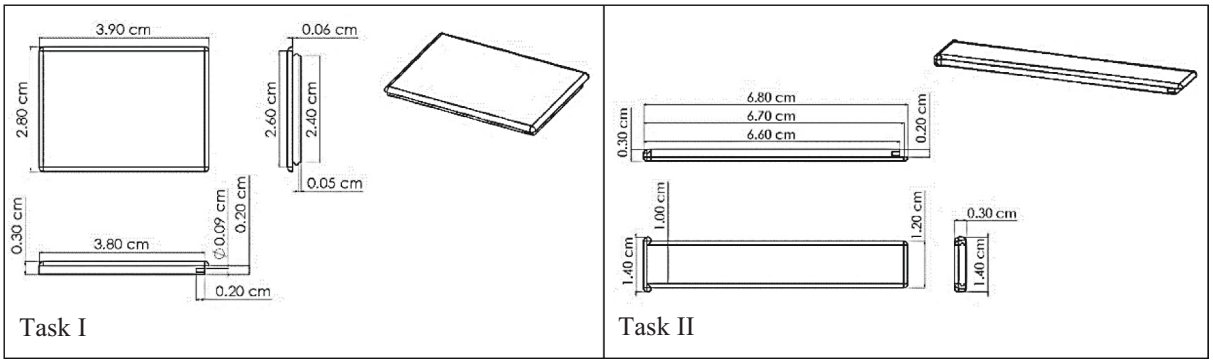

Fig. 15. Three views of printed parts in Task I and Task II.

Table 12
Parameter inputs of Task I and Task II.

Input parameters		Notations	Units	Boundaries	Values	
					Task I	Task II
Present temperatures	Present temperature of unit heating	T^0_{uh}	°C	$T^0_{uh} \leq T_{uh}$	19	41
	Present temperature of material processing	T^0_{mp}	°C	$T^0_{mp} \leq T_{mp}$	19	44
Process parameters	Target temperature of unit heating	T_{uh}	°C	[23, 80]	60	53
	Target temperature of material processing	T_{mp}	°C	[180, 250]	200	180
	Travelling speed	v_{xy}	mm/s	[10,300]	120	130
	Printing speed	v_{xy}	mm/s	[10, 150]	60	72
	Layer-switching speed	v_z	mm/s	5	5	5

Table 13
Experimental and predicted resource consumptions with percentage errors for Task I.

Resource consumption	Experimental results	Predicted results	Percentage errors
Time t (s)	3171.00	3097.69	2.31 %
Energy E (VAS)	676,928.23	651,303.61	3.79 %
Material M (g)	2.42	2.62	−8.05 %

Table 14
Experimental and predicted resource consumptions with percentage errors for Task II.

Resource consumption	Experimental results	Predicted results	Percentage errors
Time t (s)	2191.00	2020.28	7.79 %
Energy E (VAS)	398,996.29	371,078.38	7.00 %
Material M (g)	1.99	2.21	−10.65 %

7.2.3. Discussion

In the above cases, Task I printed by the Anycubic machine and Task III printed by the Monoprice machine use the same geometries with different process parameters. The different consumption levels of the two tasks indicate that machine characteristics and process parameters are the major factors affecting resource consumption. This finding further verifies the necessity of considering the above factors in prediction modelling.

According to the prediction accuracy results, the reasons for the deviations between actual and predicted consumption levels are discussed. In the actual printing process, some machine units cannot perfectly achieve the expected operations. For instance, the occurrence of stepper motor losing steps is a common problem in FDM machines. This phenomenon results from the insufficient torques and excessive loads of stepper motors, especially at a high travelling/printing speed. Thus, the actual axial moving speed is not equal to the expected speeds. In addition, according to G-codes, the expected axial motion is a uniform motion at a constant speed. In fact, there are acceleration and deceleration in each axial motion. Those machine performance levels that fall below expectations will lead to a deviation between the predicted and

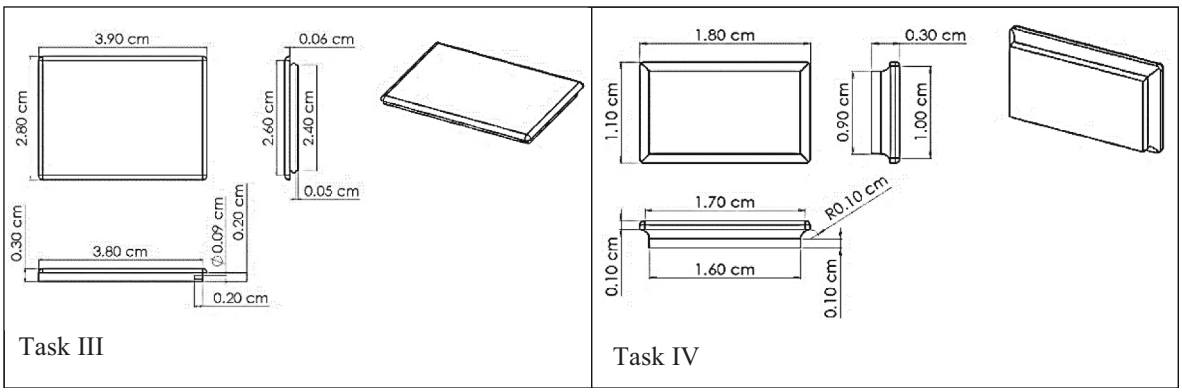

Fig. 16. Three views of the printed parts in Task III and Task IV.

Table 15
Parameter inputs of Task III and Task IV printed by the Monoprice machine.

Input parameters		Notations	Units	Boundaries	Values	
					Task III	Task IV
Present temperatures	Present temperature of unit heating	T^0_{uh}	°C	$T^0_{uh} \leq T_{uh}$	21	26
	Present temperature of material processing	T^0_{mp}	°C	$T^0_{mp} \leq T_{mp}$	34	111
Process parameters	Target temperature of unit heating	T_{uh}	°C	[23, 60]	60	47
	Target temperature of material processing	T_{mp}	°C	[180, 260]	200	182
	Travelling speed	v_{xy}	mm/s	[10, 150]	150	98
	Printing speed	v_{xy}	mm/s	[10, 150]	50	63
	Layer-switching speed	v_z	mm/s	[10, 150]	150	98

Table 16
Experimental and predicted resource consumptions with percentage errors for Task III.

Resource consumption	Experimental results	Predicted results	Percentage errors
Time t (s)	1146.00	1246.03	−8.73 %
Energy E (VAS)	97,279.55	99,869.78	−2.66 %
Material M (g)	2.24	2.82	−26.14 %

Table 17
Experimental and predicted resource consumptions with percentage errors for Task IV.

Resource consumption	Experimental results	Predicted results	Percentage errors
Time t (s)	358.00	366.87	−2.48 %
Energy E (VAS)	33,847.61	33,685.28	0.48 %
Material M (g)	0.51	0.65	−28.29 %

actual axial moving times. The above phenomenon is a major reason for the percent errors of time and energy predictions. Due to the different process parameters and part geometries, the toolpaths in the four tasks are different; therefore, the impacts of stepper motor losing steps on the prediction accuracies are different.

The stepper motor losing steps affect the prediction accuracy of material consumption due to the insufficient material feeding. On one hand, the high load and insufficient torque of high-speed printing cause the motor to lose steps; on the other hand, the insufficient melting of thermoplastic filaments at high printing speeds causes material blockage at nozzle, and the material is unable to extrude smoothly. By comparing the results, the material consumption accuracy of the Anycubic machine is better than that of the Monoprice machine. This is due to the different heating performance levels of the material processing systems (i.e., nozzle hotends). The nozzle heating efficiency of the Anycubic machine is better than that of the Monoprice machine.

The proposed modelling method can be adapted to other mainstream AM or CNC manufacturing technologies. Regardless of the type of process or material used, the manufacturing is completed through cooperative operations driven by multiple machine units with specific functions, and G-code is the commonly-used numerical control language for those manufacturing technologies. Therefore, the physical modelling based on G-codes can be generally applied to predict the time consumed for axial motions and the material consumption. The data-driven modelling requires collecting machine power and heating time, which is inevitable for predicting the energy consumption. To simplify this modelling process to the greatest extent possible, the generation of GP diagram based on G-code is necessary, which provides guidance to identify the machine operations and design experiments for the data collection. Once the predictive models for the current machine are obtained, the recourse consumption of any 3DP task to be executed can be predicted only based on the G-code file without any additional experiment.

8. Conclusion

The objective of this study is to propose a hybrid modelling scheme to predict the resource consumption of the 3DP process. The machine operations are classified into five parts: axial moving, material feeding, unit heating, material processing and auxiliary. The machine units are correspondingly classified into five subsystems. A GP diagram is generated to help understand machine behaviours. Then, the physical modelling method sufficiently utilises the manufacturing information in G-codes to model the times of axial motion and material usage. The data-driven modelling method performs experiments to measure the powers and preheating times of subsystems under different values of related process parameters and then applies the regression analysis method to regress the mathematical models. To demonstrate the prediction modelling of real-world 3DP machines, the proposed method is applied to two FDM machines. Predictive models are developed. To validate the prediction accuracy, each machine completes two printing tasks using different process parameters. The actual consumption is compared to the predicted consumption; finally, the prediction accuracies are calculated.

The outcomes of this research have the following highlights:

- The function-based classifications of machine operations and machine units are generally applicable to mainstream 3DP technologies. The model simplifies the complex and diverse machine units into five subsystems to facilitate the implementation of the proposed modelling method to any other 3DP technology.
- The generation of a GP diagram helps the understanding of machine behaviours, including the starting time of each operation, the operation sequence, and the power profiles of the 3DP machine and subsystems. This diagram provides guidance for resource consumption modelling.
- The physical modelling method based on G-codes considers the influences of process parameters on material deposition toolpaths, which is closer to the real printing process and reduces the workload of experimental measurements. The corresponding computing program can automate the G-code calculation process.
- The data-driven modelling based on experiments considers the machine characteristics and the impacts of process parameters on system power and preheating time, which is closer to the real printing process.
- In addition to 3DP, the proposed hybrid modelling method can be further expanded to other AM and CNC manufacturing technologies.

The proposed prediction modelling method is foundational. To further optimise the predictive models, additional works will be undertaken to model the actual printing/travelling speed, actual material feed, and the acceleration and deceleration of axial moving. Moreover, the prediction process will be integrated with the metaheuristic optimisation technique to guide the numerical setting of process parameters and to minimise resource consumption.

Declaration of competing interest

The authors declare that they have no known competing financial interests or personal relationships that could have appeared to influence the work reported in this paper.

Acknowledgements

This work is jointly funded by Fundamental Research Funds for the Central Universities (Grant No. 3122022QD15).

Appendix A. Experimental results of Anycubic i3 Mega FDM printer

A.1. Material processing operation

Table A.1
Experimental results of the material processing operation.

Test no.	Target temperature T_{mp} ($^{\circ}C$)	Temperature difference ΔT_{mp} ($^{\circ}C$)	Present temperature T^{0}_{mp} ($^{\circ}C$)	Preheating time t^{p}_{mp} (s)	Preheating power P^{p}_{mp} (VA)	Working power P^{w}_{mp} (VA)
1	170	63	107	30	85.87238	36.28409
2	180	49	131	24	85.88146	38.77141
3	172	54	118	25	87.02961	37.31019
4	173	69	104	31	85.10377	37.22275
5	175	81	94	35	85.69948	38.05415
6	178	83	95	36	83.20823	38.55360
7	178	86	92	36	83.49366	38.96611
8	184	92	92	38	84.04563	40.35102
9	185	94	91	39	85.40957	40.36066
10	189	96	93	40	85.68639	41.09041
11	191	114	77	45	85.48266	41.70230
12	205	121	84	49	85.61391	44.80734
13	200	128	72	50	85.97969	43.67242
14	207	137	70	53	85.84082	45.34073
15	210	142	68	54	86.94465	45.67440
16	214	149	65	59	86.81009	47.50530
17	220	152	68	60	86.41892	48.32648
18	227	160	67	64	85.17483	49.47431
19	230	163	67	65	86.27192	50.19925
20	235	174	61	69	86.93204	51.70714
21	237	177	60	71	85.76800	51.98806
22	243	183	60	73	86.76045	53.24891
23	245	186	59	75	85.79808	53.43232
24	248	190	58	76	86.37302	53.80842
25	250	198	52	78	85.80436	54.79185
Avg.					85.73614	

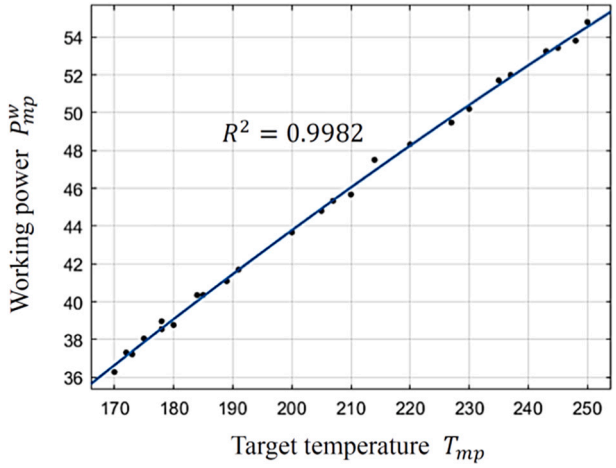

Fig. A.1. Regression curve of the working power P^{w}_{mp} and the target temperature T_{mp} for material processing

A.2. Unit heating operation

Table A.2
Experimental results of the unit heating operation.

Test No.	Target temperature T_{uh} (°C)	Temperature difference ΔT_{uh} (°C)	Present temperature T_{uh}^{0} (°C)	Preheating time t_{uh}^{p} (s)	Preheating power P_{uh}^{p} (VA)	Working power P_{uh}^{w} (VA)
1	29	3	26	11	304.61130	17.66945
2	30	4	26	11	305.60578	20.73979
3	31	7	24	21	317.60169	24.14278
4	32	5	27	16	307.15310	21.76370
5	37	8	29	27	301.99721	32.95911
6	38	9	29	26	320.41987	37.96336
7	39	10	29	31	317.31704	36.68883
8	42	12	30	42	307.83719	46.53277
9	45	13	32	46	318.47888	48.92556
10	47	14	33	52	312.41806	57.52883
11	51	18	33	67	311.24535	63.56841
12	53	20	33	83	309.65465	69.87500
13	54	23	31	92	312.70946	74.24864
14	55	25	30	103	313.00640	84.13934
15	57	26	31	108	310.11336	80.26311
16	61	28	33	123	307.94265	86.65053
17	67	29	38	139	300.54805	99.06604
18	68	30	38	143	303.95910	104.15679
19	69	33	36	174	296.25775	104.49482
20	70	36	34	175	307.61322	108.22310
21	73	37	36	185	306.45782	112.47472
22	74	38	36	189	304.80010	117.41137
23	77	39	38	210	301.66221	123.94941
24	79	40	39	216	297.45052	133.42520
25	80	46	34	248	302.19541	135.45679
Avg.					307.96224	

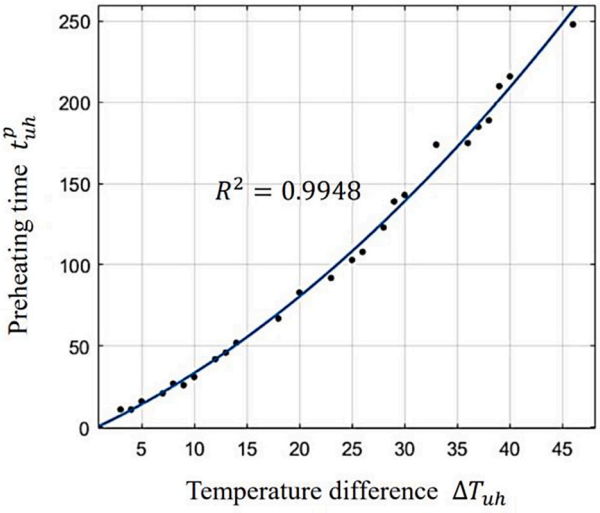

Fig. A.2. Regression curve of the preheating time t_{uh}^{p} and the temperature difference ΔT_{uh} for unit heating.

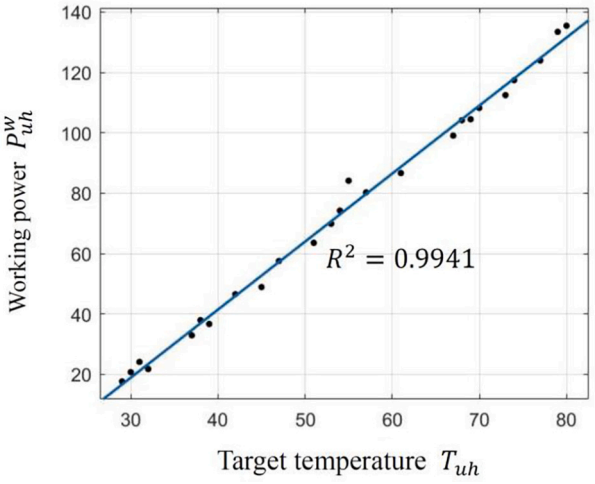

Fig. A.3. Regression curve of the working power P_{uh}^{w} and the target temperature T_{uh} for unit heating

Appendix B. Experimental results of the Monoprice MP Mini Delta FDM printer

B.1. Material processing operation

Table B.1
Experimental results of the material processing operations.

Test no.	Target temperature T_{mp} ($^{\circ}C$)	Temperature difference ΔT_{mp} ($^{\circ}C$)	Present temperature T_{mp}^{0} ($^{\circ}C$)	Preheating time t_{mp}^{p} (s)	Standby time t_{mp}^{0} (s)	Preheating power P_{mp}^{p} (VA)	Working power P_{mp}^{w} (VA)
1	150	120	30	55	27	59.82630	15.11995
2	152	40	112	27	27	58.25839	15.04325
3	159	45	114	29	26	61.85862	16.23574
4	162	52	110	32	25	62.16680	16.53417
5	169	74	95	41	24	61.28040	17.50407
6	170	96	74	50	23	61.34017	17.65508
7	174	76	98	42	22	60.44671	18.34907
8	177	86	91	46	23	60.25701	18.74738
9	190	136	54	66	19	62.06424	20.36132
10	185	94	91	50	20	60.37932	19.65971
11	187	100	87	52	20	62.20181	19.97322
12	193	109	84	56	19	61.36935	20.78699
13	197	117	80	60	18	60.37456	21.10100
14	201	119	82	61	17	60.84534	22.19950
15	205	128	77	65	17	60.56651	22.34866
16	209	137	72	69	17	60.70359	22.80714
17	210	160	50	76	15	62.31859	23.16485
18	218	138	80	70	14	60.70939	24.24879
19	224	149	75	76	12	60.63197	24.92717
20	236	156	80	81	10	60.83663	26.70383
21	241	164	77	84	9	61.35182	27.44286
22	247	167	80	87	7	60.83855	28.05785
23	252	172	80	90	6	62.03977	29.69533
24	258	180	78	94	3	64.16866	28.74100
25	260	203	57	103	0	61.34960	30.47362
Avg.						61.12736	

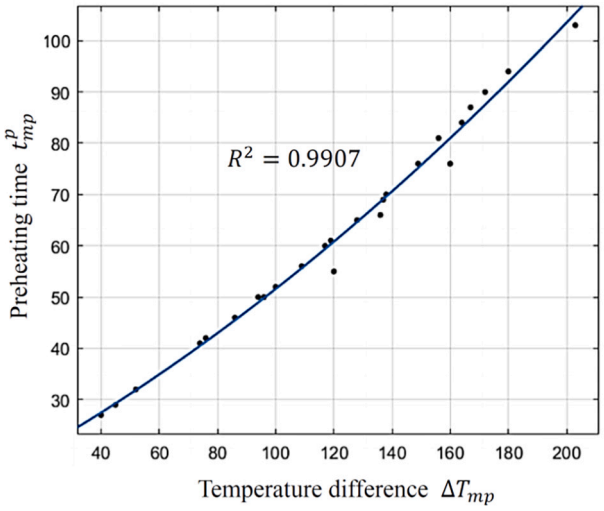

Fig. B.1. Regregression curve of the preheating time t^p_{mp} and the temperature difference ΔT_{mp} for material processing.

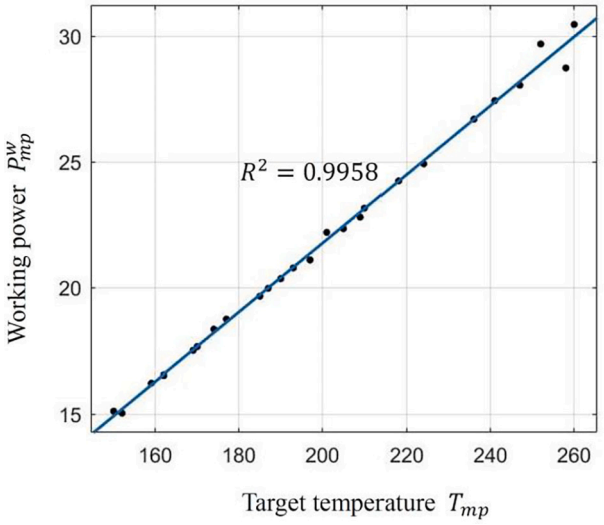

Fig. B.2. Regression curve of the working power P^w_{mp} and the target temperature T_{mp} for material processing

B.2. Unit heating operation

Table B.2
Experimental results of the unit heating operation.

Test no.	Target temperature T_{uh} (°C)	Temperature difference ΔT_{uh} (°C)	Present temperature T^0_{uh} (°C)	Preheating time t^p_{uh} (s)	Preheating power P^p_{uh} (VA)	Working power P^w_{uh} (VA)
1	25	2	23	69	14.10278	8.12858
2	26	3	23	75	14.82010	9.40975
3	28	5	23	96	16.43614	13.11803
4	30	6	24	105	17.26146	10.44747
5	31	7	24	100	17.52529	10.87826
6	33	7	26	116	18.41851	11.37769
7	35	8	27	114	20.93038	11.80378
8	38	9	29	107	24.44937	13.91109
9	39	9	30	105	23.41795	16.25311
10	40	10	30	112	24.75183	13.52668
11	41	11	30	116	24.29871	17.12859
12	44	12	32	139	24.25617	15.92876
13	45	14	31	140	24.64510	16.72144
14	47	15	32	153	26.77658	17.91362
15	48	18	30	150	27.66501	18.62048
16	50	20	30	169	28.35524	19.40375

(*continued on next page*)

Table B.2 (*continued*)

Test no.	Target temperature T_{uh} ($^{\circ}C$)	Temperature difference ΔT_{uh} ($^{\circ}C$)	Present temperature T_{uh}^{0} ($^{\circ}C$)	Preheating time t_{uh}^{p} (s)	Preheating power P_{uh}^{p} (VA)	Working power P_{uh}^{w} (VA)
17	51	23	28	180	28.53120	20.05380
18	53	24	29	184	31.94140	21.61581
19	54	26	28	196	30.76732	22.12246
20	55	28	27	204	32.38990	22.66014
21	56	30	26	206	33.30020	22.81804
22	57	32	25	211	34.28504	23.69356
23	58	34	24	222	35.04665	24.15118
24	59	38	21	222	38.05697	27.45379
25	60	40	20	225	36.66811	25.27205

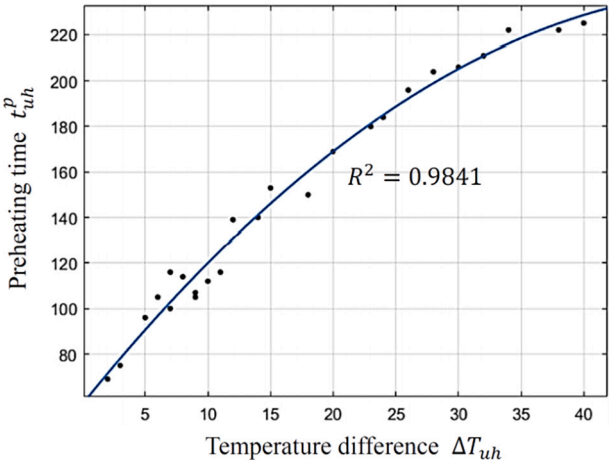

Fig. B.3. Regression curve of the preheating time t_{uh}^{p} and the temperature difference ΔT_{uh} for unit heating.

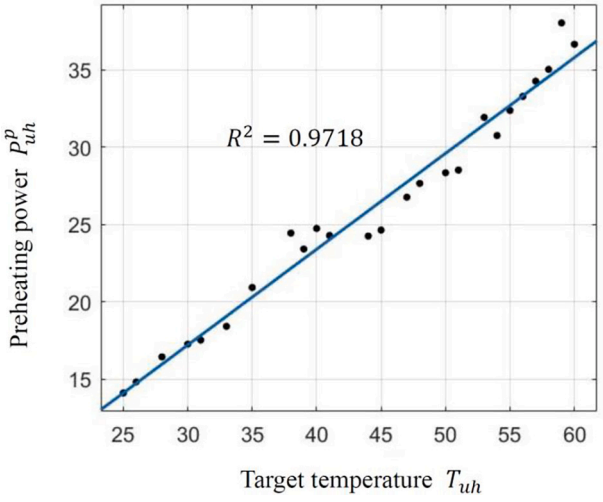

Fig. B.4. Regression curve of the preheating power P_{uh}^{p} and the target temperature T_{uh} for unit heating.

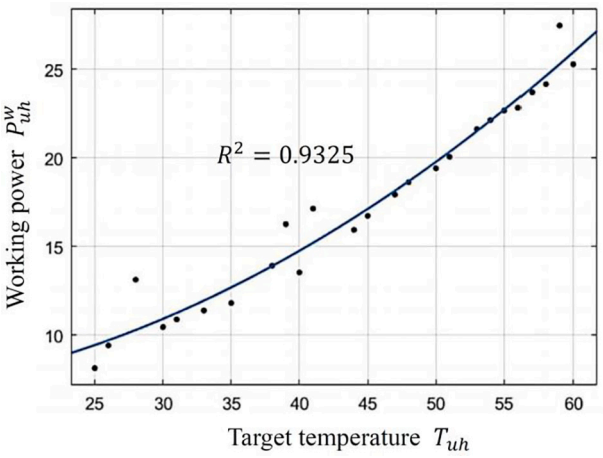

Fig. B.5. Regression curve of the working power P_{uh}^w and the target temperature T_{uh} for unit heating.

References

[1] Tamez MBA, Taha I. A review of additive manufacturing technologies and markets for thermosetting resins and their potential for carbon fiber integration. Addit Manuf 2021;37:101748. https://doi.org/10.1016/j.addma.2020.101748.

[2] Yadav D, Garg RK, Ahlawat A, Chhabra D. 3D printable biomaterials for orthopedic implants: solution for sustainable and circular economy. Resour Policy 2020;68:101767. https://doi.org/10.1016/j.resourpol.2020.101767.

[3] Eyers DR, Potter AT. Industrial additive manufacturing: a manufacturing systems perspective. Comput Ind 2017;92:208–18. https://doi.org/10.1016/j.compind.2017.08.002.

[4] Gleadall A. FullControl GCode designer: open-source software for unconstrained design in additive manufacturing. Addit Manuf 2021;46:102109. https://doi.org/10.1016/j.addma.2021.102109.

[5] Yang J, Chen Y, Huang W, Li Y. Survey on artificial intelligence for additive manufacturing. In: 2017 23rd International Conference on Automation and Computing (ICAC); 2017. https://doi.org/10.23919/IConAC.2017.8082053.

[6] Chhabra D, Deswal S, Kaushik A, Garg RK, Kovács A, Khargotra R, et al. Analysis of fused filament fabrication parameters for sliding wear performance of carbon reinforced polyamide composite material fabricated parts using a hybrid heuristic tool. Polym Test 2023;118:107910. https://doi.org/10.1016/j.polymertesting.2022.107910.

[7] Yadav D, Chhabra D, Gupta RK, Phogat A, Ahlawat A. Modeling and analysis of significant process parameters of FDM 3D printer using ANFIS. Mater Today: Proc 2020;21:1592–604. https://doi.org/10.1016/j.matpr.2019.11.227.

[8] Yadav D, Chhabra D, Garg RK, Ahlawat A, Phogat A. Optimization of FDM 3D printing process parameters for multi-material using artificial neural network. Mater Today: Proc 2020;21:1583–91. https://doi.org/10.1016/j.matpr.2019.11.225.

[9] Sharma A, Chhabra D, Sahdev R, Kaushik A, Punia U. Investigation of wear rate of FDM printed TPU, ASA and multi-material parts using heuristic GANN tool. Mater Today: Proc 2022;63:559–65. https://doi.org/10.1016/j.matpr.2022.04.015.

[10] Duflou J, Kellens K. Cleaner production. In: CIRP Encyclopedia of Production Engineering; 2016. p. 1–4. https://doi.org/10.1007/978-3-642-35950-7_6635-3.

[11] Kellens K, Baumers M, Gutowski TG, Flanagan W, Lifset R, Duflou JR. Environmental dimensions of additive manufacturing. Mapping application domains and their environmental implications. Environ Dimens Addit Manuf 3D Print 2017;21:S49–68. https://doi.org/10.1111/jiec.12629.

[12] Yoon HS, Lee JY, Kim HS, Kim MS, Kim ES, Shin YJ, et al. A comparison of energy consumption in bulk forming, subtractive, and additive processes: review and case study. Int J Precis Eng Manuf - Green Technol 2014;1:261–79. https://doi.org/10.1007/s40684-014-0033-0.

[13] Kumar MB, Sathiya P. Methods and materials for additive manufacturing: a critical review on advancements and challenges. Thin Wall Struct 2020;159:107228. https://doi.org/10.1016/j.tws.2020.107228.

[14] Han M, Yang MY, Li L. Energy consumption modeling of 4D printing thermal-responsive polymers with integrated compositional design for material. Addit Manuf 2020;34:101223. https://doi.org/10.1016/j.addma.2020.101223.

[15] Baumers M, Tuck C, Wildman R, Ashcroft I, Rosamond E, Hague R. Transparency built-in: energy consumption and cost estimation for additive manufacturing. J Ind Ecol 2013;17:418–31. https://doi.org/10.1111/j.1530-9290.2012.00512.x.

[16] Zhang Y, Bernard A. Generic build time estimation model for parts produced by SLS. In: Proceedings of the 6th International Conference on Advanced Research in Virtual and Rapid Prototyping; 2016. https://doi.org/10.1201/b15961-10.

[17] Campbell I, Combrinck J, de Beer D, Barnard L. Stereolithography build time estimation based on volumetric calculations. Rapid Prototyping J 2008;14:271–9. https://doi.org/10.1108/13552540810907938.

[18] Munguía J, Ciurana J, Riba C. Neural-network-based model for build-time estimation in selective laser sintering. P I Mech Eng B-J Eng 2009;223:995–1003. https://doi.org/10.1243/09544054JEM1324.

[19] Zhang Y, Bernard A, Valenzuela JM, Karunakaran K. Fast adaptive modeling method for build time estimation in additive manufacturing. CIRP J Manuf Sci Tec 2015;10:49–60. https://doi.org/10.1016/j.cirpj.2015.05.003.

[20] Sreenivasan R, Bourell D. Sustainability study in selective laser sintering - an energy perspective. In: 20th Annual International Solid Freeform Fabrication Symposium; 2009.

[21] Baumers M, Tuck C, Bourell DL, Sreenivasan R, Hague R. Sustainability of additive manufacturing: measuring the energy consumption of the laser sintering process. P I Mech Eng B-J Eng 2011;225:2228–39. https://doi.org/10.1177/0954405411406044.

[22] Meteyer S, Xu X, Perry N, Zhao YF. Energy and material flow analysis of binder-jetting additive manufacturing processes. Procedia CIRP 2014;15:19–25. https://doi.org/10.1016/j.procir.2014.06.030.

[23] Li YA, Bahram B, Jan CA. Development and validation of an energy simulation for a desktop additive manufacturing system. Addit Manuf 2020;32:101021. https://doi.org/10.1016/j.addma.2019.101021.

[24] Lunetto V, Galati M, Settineri L, Iuliano L. Unit process energy consumption analysis and models for Electron Beam Melting (EBM): effects of process and part designs. Addit Manuf 2020;33:101115. https://doi.org/10.1016/j.addma.2020.101115.

[26] Yang J. A multi-objective prediction and optimisation method for additive manufacturing technology [Ph.D. thesis],. University of Glasgow; 2021.

[27] Smid P. CNC Programming Handbook: a Comprehensive Guide to Practical CNC Programming. Industrial Press Inc; 2003. p. 47–92.

[28] Smid P. CNC Control Setup for Milling and Turning: Mastering CNC Control Systems. Industrial Press Inc; 2010. p. 261–3.

[29] Jenkins DG, Quintana-Ascencio PF. A solution to minimum sample size for regressions. PloS One 2020;15:e0229345. https://doi.org/10.1371/journal.pone.0229345.

[30] El-Habrouk M, Darwish M, Mehta P. Active power filters: a review. IET Electr Power App 2000;147:403–13. https://doi.org/10.1049/ip-epa:20000522.

[31] Curve Fitting Toolbox. Uk.Mathworks.com. https://uk.mathworks.com/products/curvefitting/;; 2022 [accessed 02 August 2022].

[32] Yeh AB. Review of a modern introduction to probability and statistics, by Dekking FM, Kraaikamp C, Lopuhaa HP. Meester LE Technometrics 2007;49:359. http://www.jstor.org/stable/25471355.

[33] i3 Mega S. ANYCUBIC 3D Printing. https://www.anycubic.com/products/anycubic-i3-mega-s/;; 2022 [accessed 02 August 2022].

[34] Mini Delta 3D Printer | UK Version. Monoprice United Kingdom. https://www.monoprice.uk/collections/3d-printers/products/monoprice-mp-mini-delta-3d-printer-uk-open-box/;; 2022 [accessed 02 August 2022].